J. Fluid Mech. (1994), *vol.* 263, *pp.* 151–183

Roll waves on a shallow layer of mud modelled as a power-law fluid

By CHIU-ON NG AND CHIANG C. MEI

Department of Civil and Environmental Engineering, Massachusetts Institute of Technology, Cambridge, MA 02139, USA

(Received 20 April 1993 and in revised form 13 September 1993)

We give a theory of permanent roll waves on a shallow layer of fluid mud which is modelled as a power-law fluid. Based on the long-wave approximation, Kármán's momentum integral method is applied to derive the averaged continuity and the momentum equations. Linearized instability analysis of a uniform flow shows that the growth rate of unstable disturbances increases monotonically with the wavenumber, and therefore is insufficient to suggest a preferred wavelength for the roll wave. Nonlinear roll waves are obtained next as periodic shocks connected by smooth profiles with depth increasing monotonically from the rear to the front. Among all wavelengths only those longer than a certain threshold correspond to positive energy loss across the shock, and are physically acceptable. This threshold also implies a minimum discharge, viewed in the moving system, for the roll wave to exist. These facts suggest that a roll wave developed spontaneously from infinitesimal disturbances should have the shortest wavelength corresponding to zero dissipation across the shock, though finite dissipation elsewhere. The discontinuity at the wave front is a mathematical shortcoming needing a local requirement. Predictions for the spontaneously developed roll waves in a Newtonian case are compared with available experimental data. Longer roll waves, with dissipation at the discontinuous fronts, cannot be maintained if the uniform flow is linearly stable, when the fluid is slightly non-Newtonian. However, when the fluid is highly non-Newtonian, very long roll waves may still exist even if the corresponding uniform flow is stable to infinitesimal disturbances. Numerical results are presented for the phase speed, wave height and wavenumber, and wave profiles for a representative value of the flow index of fluid mud.

1. Introduction

It has been known for a long time that a steady discharge of water into a long open channel frequently develops into a series of progressing bores (Cornish 1934). These bores are sandwiched between long stretches of gentle profiles increasing monotonically in depth from rear to front. The wave system is called roll waves.

In muddy rivers intermittent flows of clay/water mixture are also frequent, especially after torrential rain. Mud flows resulting from volcano eruptions can also be accompanied by intermittent waves. Observations of these waves have been reported for Wrightwood in California (Sharp & Nobles 1953; Johnson 1970), Mt Thomas in New Zealand (Pierson 1980), Mt Yakedake in Japan (Okuda *et al.* 1980), Jiang-jia Ravine in Southwest China (Li *et al.* 1983) and tributaries of Yellow River in China (Wan, 1982). In Jiang-jia Ravine which is a gully about 20–25 m in width, the mud flow surges down during the wet season in groups of successive bores. The maximum wave

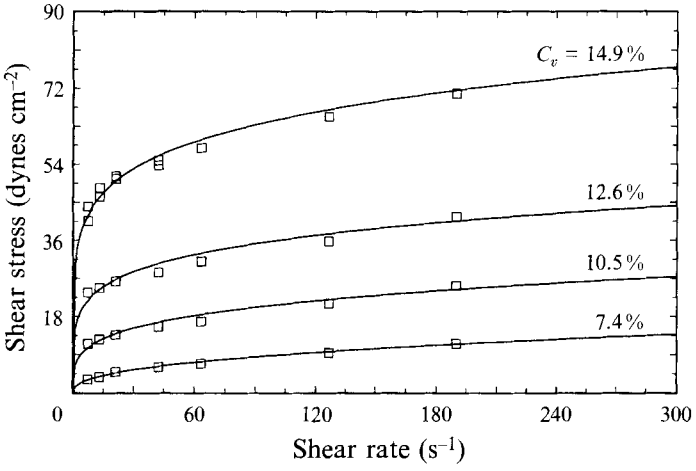

FIGURE 1. Fitting of the power-law model to the rheological data measured by Wan (1982) for kaolinite suspension.

height once reached 4 m and the maximum wave velocity 13 m s^{-1}, while the discharge per wave was as much as 2420 m^3 s^{-1}. The wavelength varied between 20 and 100 m, while the period of each wave ranged from 5 to 60 s. The bore fronts splattered with so much force that even large stones were thrown into the air. The flow in the rear of the waves was however much shallower, slower and essentially laminar, and frequently stagnant before the next surge. Such intermittent mud flows are responsible for the severe erosion and deposition of bed materials in Jiang-jia Ravine.

Theoretically roll waves were first analysed for clear water in open channels by Jeffreys (1925) as a problem of linearized instability of a steady turbulent current. The mathematical theory for roll waves of finite amplitude was later given by Dressler (1949) who fitted shocks between periodic stretches of smooth profiles. In Dressler's theory, given the values of the slope and the roughness, one must also specify the wave speed and length, in order to determine all other flow characteristics such as shock amplitude and flow velocity and depth. He also showed the existence of a critical section where both the numerator and the denominator of the profile equation vanish. In addition, Dressler found that roll waves will occur only if the bottom roughness of the channel is non-zero and less than a certain critical value, as required by the instability criterion for a linearized disturbance.

Dressler's theory of roll waves was extended to laminar water flows by Ishihara, Iwagaki & Iwasa (1954), who also carried out experiments in a thin sheet of water. Tamada & Tougou (1979) studied the linearized instability of the nonlinear laminar roll waves of Ishihara *et al.*, and solved numerically an eigenvalue problem. To determine the roll wavelength, they searched for the length of the 'most stable' wave which corresponds to the eigenvalue with the fastest decay rate. Their mathematical procedure was however not sufficiently clear to be convincing. Experiments on laminar roll waves have also been conducted in an open channel by Mayer (1959), with particular emphasis on the initial development of roll waves near the entrance of a long channel. Similar experiments have been performed more recently by Julien & Hartley (1985, 1986). Again attention was focused on the formation length of roll waves on an incline. Linear and nonlinear waves of continuous profile on a Newtonian thin film with strong surface tension is a much studied subject; for recent developments and the extensive bibliography, reference should be made to Needham & Merkin (1984),

Alekseenko, Nakoryakov & Pokusaev (1985), Merkin & Needham (1986), Hwang & Chang (1987), Needham (1988, 1990), Prokopiou, Cheng & Chang (1991), Chang, Demekhin & Kopelevich (1993) and Liu, Paul & Gollub (1993).

Without or without bores, intermittent mud or debris flows can be laminar except near the bore front because of the high viscosity (Johnson 1970; Davies 1986). The problem of roll waves in laminar flow of non-Newtonian fluids has only been studied by Liu (1990) who examined the rapid flow of Bingham-plastic fluids down an incline. Under certain conditions, the growth rate of unstable wave may have a maximum for a certain wavelength. Taking the most unstable infinitesimal progressive wave as the initial disturbance, Liu calculated numerically the transient development into periodic shocks in a thin layer of Bingham-plastic mud flow.

The Bingham model is however a mathematical idealization. At low shearing rates (5–50 s^{-1}), the rheological character of thick fluid mud is known to be shear thinning (e.g. see Wan 1982; Kajiuchi & Saito 1984; O'Brien & Julien 1988). It is also known that in the field the shearing rate is often less than 100 s^{-1} (Qian & Wan 1986; Johnson 1970; Yano & Daido 1985). In a transient theory the Bingham model also poses difficulties because of the presence of the yield surface along which the shear stress equals the yield stress. The position of the yield surface is not known *a priori* and has to be solved as a part of the transient nonlinear problem.

At low shear rates, a more appropriate and convenient model is the power law which reads, in simple shear,

$$\tau = \mu_n \left(\frac{\partial u}{\partial z}\right)^n, \tag{1.1}$$

where μ_n is the viscosity coefficient of dimension $[ML^{-1}T^{n-2}]$, and n is the flow index which is between 0 and 1 for a shear-thinning fluid. The special limit of $n = 1$ corresponds to a Newtonian fluid, and μ_1 is the ordinary dynamic viscosity. In figure 1, we show how the power-law model fits the measured relation between the shear stress and the strain rate data for a kaolinite suspension measured by Wan (1982). For these data, the parameters μ_n and n may be expressed in terms of the volume concentration C_v by

$$\mu_n = 1.86 \times 10^{-4} C_v^{4.45}, \tag{1.2}$$

$$n = 5.86 C_v^{-1.34}, \tag{1.3}$$

where μ_n is in dynes cm^{-2} s^n, and C_v is a percentage. It can be seen that μ_n increases while n decreases with the volume concentration. A similar trend of change of the power-law parameters with the volume concentration is also reported by Dai *et al.* (1980) and Darby (1986). Figure 2 has been compiled to give the empirical relation between n and the volume concentration from the following sources: Wan (1982) for kaolinite suspension; Bryant & Williams (1980) for Brisbane mud and Rotterdam mud; Darby (1986) for pulverized lignite suspension in saline water; Dai *et al.* (1980) for slurry mud; and Tanner (1985) for cement rocks in water. The fact that the data points are scattered suggests that other factors such as chemical composition and particle sizes may also be influential. In any case it may be noted that for the same type of solid content, n decreases as the concentration increases. The data points lie in the range $0.1 \leqslant n \leqslant 0.4$ for volume concentrations below 60%.

For the flow to remain laminar, it is necessary that the Reynolds number be below certain threshold: $Re < Re_c$. For power-law fluids, Darby (1986) gave the following empirical relation for circular pipe flows:

$$Re_{(pipe)} < Re_{c(pipe)} = 0.125 \left[\frac{2(1+3n)}{n}\right]^n [2100 + 875(1-n)], \tag{1.4}$$

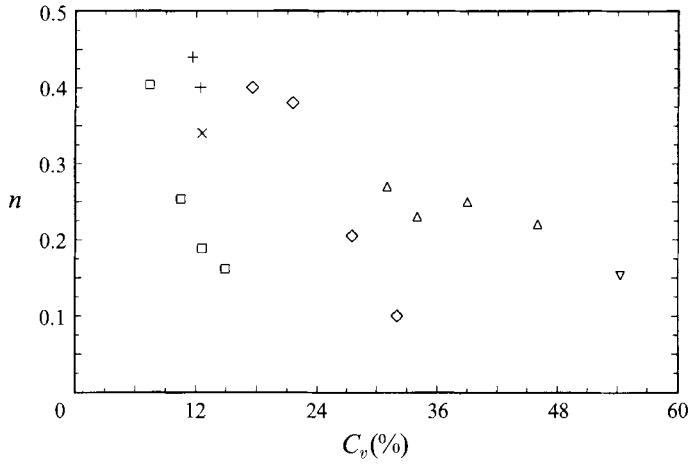

FIGURE 2. Correlation of n with C_v for various solid compositions: □, kaolinite suspension (Wan 1982); ×, Rotterdam mud (Bryant & Williams 1980); +, Brisbane mud (Bryant & Williams 1980); △, lignite suspension (Darby 1986); ◇, slurry (Dai *et al.* 1980); ▽, cement rock in water (Tanner 1985).

n	1.0	0.4	0.1
C_v (%)	0	7.4	20.9
ρ (kg m^{-3})	1000	1120	1340
μ_n (Pa s^n)	0.001	0.14	13.8
Re_c	525	492	435
$\theta = 0.001$ rad.			
Q_c (m^2 s^{-1})	5.3×10^{-4}	0.0188	3.0397
h_c (m)	0.0054	0.0512	1.4054
$\bar{u}_c$ (m s^{-1})	0.0966	0.3679	2.1628
$\theta = 0.1$ rad.			
Q_c (m^2 s^{-1})	5.3×10^{-4}	0.0019	0.0588
h_c (m)	0.0012	0.0024	0.0218
$\bar{u}_c$ (m s^{-1})	0.4481	0.7924	2.6929

TABLE 1. Flow parameters for various n, and physical discharge rates, depths and mean velocities for two slopes θ

where
$$Re_{(pipe)} \equiv \frac{\rho \bar{u}^{2-n} D^n}{\mu_n} \tag{1.5}$$

while $\bar{u}$ and D denote the mean velocity and the pipe diameter respectively. As is customary in the hydraulics of wide open channels, D is replaced by 4 times the channel depth. Therefore (1.4) is rewritten as

$$Re = \frac{\rho \bar{u}^{2-n} h^n}{\mu_n} < Re_c = 0.125 \left(\frac{1+3n}{2n}\right)^n [2100 + 875(1-n)]. \tag{1.6}$$

From (1.6), the upper bounds Re_c for $n = (1.0, 0.4, 0.1)$ are respectively $Re_c = (525, 492, 435)$. As a numerical example, we compare the uniform flow of a power-law fluid mud with clear water of $n = 1.0$. For the two slopes $\theta = 0.001$, 0.1 rad., the physical discharge rates, depths and mean velocities (with a subscript c) corresponding to the

above three upper limits are calculated according to (2.10) and (2.11) and presented in table 1.

Note that, at a mild slope, the depth of a Newtonian fluid must be of the order of millimeters, while that of the highly non-Newtonian fluid can be 1 m or more, for the flow to remain laminar. Taking the example of Jiang-jia Ravine, we cite the following data from Li *et al.* (1983) for one particular mud flow: $\rho = 2130$ kg m^{-3}, $\sin\theta = 0.06$, $h = 1.40$ m, surface velocity $u(h) = 8.0$ m s^{-1}. Li *et al.* chose the Bingham model and estimated the yield strength of the mud to be 2000–3000 dynes cm^{-2}. Their measured Bingham viscosity is in the order of 30 P.† From these Bingham model parameters, we fit a power-law model with: $n = 0.3$ and $\mu_n = 150$ Pas^n. Hence the depth-averaged velocity $\bar{u}$, which is given by (2.9), equals $\frac{1.3}{1.6}u(h) = 6.5$ m s^{-1}. The Reynolds number may now be calculated:

$$Re = \frac{\rho \bar{u}^{2-n} h^n}{\mu_n} = \frac{2130 \times 6.5^{1.7} \times 1.4^{0.3}}{150} = 379.$$

The corresponding threshold is $Re_c = 479$. The mud flow in Jiang-jia Ravine is therefore laminar despite its relatively high velocity.

In this paper we shall develop a theory for stationary roll waves in laminar flow of a power-law fluid layer down an incline. Dissipation is present in the laminar part as well as inside the bores where there must be local turbulence. The long-wave approximation is invoked first. By a linearized instability analysis, it is shown that the growth rate of the unstable waves possesses no maximum with respect to the wavenumber. The main part is on the profile of the roll wave presented in §5. Energy loss rate at the shock is calculated. It is found that the shock amplitude must exceed a non-zero threshold in order for the loss to be positive. This threshold corresponds to a roll wave with only laminar dissipation, and the shortest wavelength. It is argued that these roll waves are the most likely to arise spontaneously from instability. Numerical results for these and longer roll waves are discussed.

2. Long-wave approximation

Consider a two-dimensional laminar flow of a thin layer of mud down a plane of inclination θ which can be any positive value not greater than 90°. An (x, z) coordinate system is defined with the x-axis along and the z-axis normal to the plane bed. The longitudinal and transverse velocity components are denoted by $u, v(x, z, t)$, the pressure by $p(x, z, t)$, and the depth normal to the bed by $h(x, t)$. Following long-wave expansions, the equations of motion are approximated as follows:

$$\frac{\partial u}{\partial x} + \frac{\partial v}{\partial z} = 0, \tag{2.1}$$

$$\frac{\partial u}{\partial t} + u\frac{\partial u}{\partial x} + v\frac{\partial u}{\partial z} = -\frac{1}{\rho}\frac{\partial p}{\partial x} + g\sin\theta + \frac{1}{\rho}\frac{\partial \tau_{zx}}{\partial z}, \tag{2.2}$$

$$0 = -\frac{1}{\rho}\frac{\partial p}{\partial z} - g\cos\theta, \tag{2.3}$$

† Li *et al.* also estimated the Bingham viscosity according to the Newtonian theory $\mu = \rho g \sin\theta h^2/(2u(h))$. Using the total depth for h, they found $\mu = 1500$ P which is far greater than the measured value. The consistent estimate should be based on the depth h_y of the sheared zone where the shear stress exceeds the yield stress. This implies that h_y is approximately equal to $0.15h$.

where ρ is the fluid density and g is the gravitational acceleration. The boundary conditions are

$$u = v = 0 \quad \text{at} \quad z = 0, \tag{2.4}$$

$$v = \frac{\partial h}{\partial t} + u\frac{\partial h}{\partial x} \quad \text{at} \quad z = h, \tag{2.5}$$

$$p = 0, \quad \frac{\partial u}{\partial z} = 0 \quad \text{at} \quad z = h. \tag{2.6}$$

Equations (2.3) and (2.6) imply that the pressure is hydrostatic:

$$p = \rho g \cos\theta (h - z). \tag{2.7}$$

These approximate equations can be deduced in the usual manner by proper scaling. Under the assumptions of long waves and high Reynolds number, (2.1)–(2.7) represent the leading-order results in a perturbation analysis. This is sketched in Appendix A.

Inserting (1.1) and (2.7) into (2.2), the x-momentum equation reads

$$\frac{\partial u}{\partial t} + u\frac{\partial u}{\partial x} + v\frac{\partial u}{\partial z} = g\left(\sin\theta - \cos\theta\frac{\partial h}{\partial x}\right) + \frac{\mu_n}{\rho}\frac{\partial}{\partial z}\left(\frac{\partial u}{\partial z}\right)^n. \tag{2.8}$$

The limiting velocity profile for a steady uniform flow is obtainable from (2.8):

$$u(z) = \frac{1+2n}{1+n}\bar{u}\left[1 - \left(1 - \frac{z}{h}\right)^{\frac{1+n}{n}}\right], \tag{2.9}$$

where $\bar{u}$ is the depth-averaged velocity

$$\bar{u} \equiv h^{-1}\int_0^h u(z)\,\mathrm{d}z = \frac{n}{1+2n}\left(\frac{\rho g \sin\theta}{\mu_n} h^{1+n}\right)^{\frac{1}{n}}. \tag{2.10}$$

Profiles of $u(z)/\bar{u}$ for $n = 1$, 0.4 and 0.1 are plotted in figure 3. The presence of a near-plug flow zone for the non-Newtonian case is evident for small n. The steady discharge rate per unit width is

$$Q = \bar{u}h = \frac{n}{1+2n}\left(\frac{\rho g \sin\theta}{\mu_n}\right)^{\frac{1}{n}} h^{\frac{1+2n}{n}}. \tag{2.11}$$

It is clear that in a steady uniform flow of known fluid properties, any two of the four parameters $(Q, h, \bar{u}, \theta)$ define the flow.

For long waves, variation in the longitudinal direction must be slow; we therefore apply Kármán's momentum integral method by assuming that (2.9) is also true for $u(x, z, t)$ in a transient and non-uniform flow, but with $\bar{u}$ and h dependent on x and t. In the Newtonian case, (2.9) is a parabolic profile. Integrating (2.1) and (2.8) with respect to z from 0 to h and using the Leibniz rule, we get

$$\frac{\partial}{\partial x}\int_0^h u\,\mathrm{d}z - u(h)\frac{\partial h}{\partial x} + v(h) - v(0) = 0, \tag{2.12}$$

$$\frac{\partial}{\partial t}\int_0^h u\,\mathrm{d}z - u(h)\frac{\partial h}{\partial t} + \frac{\partial}{\partial x}\int_0^h u^2\,\mathrm{d}z - u^2(h)\frac{\partial h}{\partial x} + u(h)\,v(h) - u(0)\,v(0)$$

$$= g\left(\sin\theta - \cos\theta\frac{\partial h}{\partial x}\right)h + \frac{\mu_n}{\rho}\int_0^h \frac{\partial}{\partial z}\left(\frac{\partial u}{\partial z}\right)^n \mathrm{d}z. \tag{2.13}$$

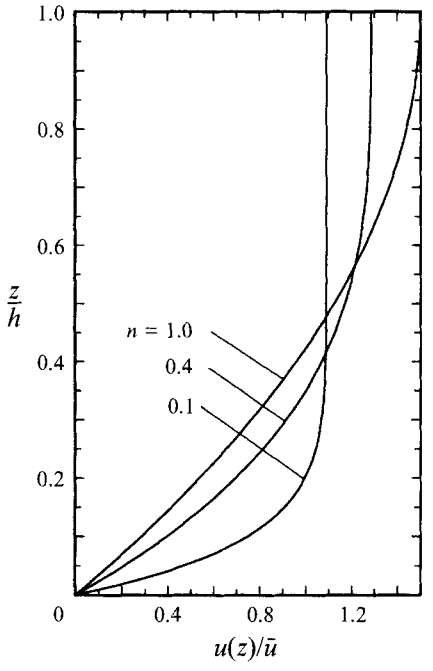

FIGURE 3. Velocity profiles for $n = 1.0$, 0.4 and 0.1.

By the boundary conditions (2.4) and (2.5) and the velocity profile (2.9), we may simplify (2.12) and (2.13) to

$$h_t + (\bar{u}h)_x = 0, \tag{2.14}$$

$$(\bar{u}h)_t + (\beta \bar{u}^2 h + \tfrac{1}{2}\cos\theta g h^2)_x = \sin\theta g h - \frac{\mu_n}{\rho}\left[\frac{1+2n}{n}\frac{\bar{u}}{h}\right]^n, \tag{2.15}$$

where β is the momentum flux factor

$$\beta \equiv (\bar{u}^2 h)^{-1}\int_0^h u^2\,\mathrm{d}z = \frac{2(1+2n)}{(2+3n)}. \tag{2.16}$$

For shear-thinning fluids, $0 < n \leqslant 1$; the range for β is

$$1 < \beta \leqslant \tfrac{6}{5}. \tag{2.17}$$

The bottom stress follows by putting (2.9) into (1.1) and setting $z = 0$:

$$\tau_b = \mu_n\left[\left(\frac{1+2n}{n}\right)\frac{\bar{u}}{h}\right]^n. \tag{2.18}$$

For Newtonian layers the momentum integral method has been employed before by Kapitza (1948), Ishihara *et al.* (1954), Alekseenko *et al.* (1985), and Prokopiou *et al.* (1991). It is well known in boundary-layer theory that the momentum integral method is a method of moments which may give numerically different but acceptable results for the global quantities if different velocity profiles are assumed. Therefore the qualitative behaviour of the global result such as the wall stress in the Blasius problem can still be crudely predicted (Schlichting 1979). It is reasonable to expect (2.9) to be useful away from the shock but not very near the shock where rapid changes in x and z must occur.

3. Normalization

We shall suppose that the spatially averaged discharge rate is known:

$$\langle Q\rangle \equiv \lambda^{-1}\int_0^{\lambda} Q(\xi)\,\mathrm{d}\xi, \tag{3.1}$$

where λ is the wavelength. In terms of $\langle Q\rangle$, a characteristic depth h_0 and a characteristic velocity $\bar{u}_0$ may be defined in the manner of (2.10) and (2.11):

$$h_0 = \left(\frac{1+2n}{n}\right)^{\frac{n}{1+2n}}\left(\frac{\mu_n}{\rho g\sin\theta}\right)^{\frac{1}{1+2n}}\langle Q\rangle^{\frac{n}{1+2n}} \tag{3.2}$$

and

$$\bar{u}_0 = \left(\frac{n}{1+2n}\right)^{\frac{n}{1+2n}}\left(\frac{\rho g\sin\theta}{\mu_n}\right)^{\frac{1}{1+2n}}\langle Q\rangle^{\frac{1+n}{1+2n}}$$

$$= \frac{n}{1+2n}\left(\frac{\rho g\sin\theta}{\mu_n}\right)^{\frac{1}{n}} h_0^{\frac{1+n}{n}}, \tag{3.3}$$

so that

$$\langle Q\rangle = \bar{u}_0 h_0. \tag{3.4}$$

In Newtonian fluids, (3.2) and (3.3) are known respectively as the Nusselt thickness and the Nusselt velocity.

In terms of h_0 and $\bar{u}_0$, we further define a characteristic bottom stress according to (2.18):

$$\tau_{b0} = \mu_n\left[\left(\frac{1+2n}{n}\right)\frac{\bar{u}_0}{h_0}\right]^n. \tag{3.5}$$

We also introduce a longitudinal lengthscale

$$l_0 = \frac{\bar{u}_0^2}{g\sin\theta} \tag{3.6}$$

and define normalized quantities (marked with an asterisk) as follows:

$$x = l_0 x^*, \quad (h,z) = h_0(h^*,z^*), \quad t = \frac{l_0}{\bar{u}_0}t^*, \tag{3.7a}$$

$$\bar{u} = \bar{u}_0\bar{u}^*, \quad Q = (\bar{u}_0 h_0)Q^*, \quad \tau_b = \tau_{b0}\tau_b^*. \tag{3.7b}$$

In dimensionless form, (2.14), (2.15) and (2.18) become

$$h_{t^*}^* + (\bar{u}^*h^*)_{x^*} = 0, \tag{3.8}$$

$$(\bar{u}^*h^*)_{t^*} + (\beta\bar{u}^{*2}h^* + \tfrac{1}{2}\alpha h^{*2})_{x^*} = h^* - \left(\frac{\bar{u}^*}{h^*}\right)^n, \tag{3.9}$$

$$\tau_b^* = \left(\frac{\bar{u}^*}{h^*}\right)^n. \tag{3.10}$$

To arrive at (3.9), use has been made of (3.3) and

$$\alpha \equiv \frac{\cos\theta g h_0}{\bar{u}_0^2}. \tag{3.11}$$

Further utilizing (3.3), we may write

$$\alpha = \left(\frac{1+2n}{n}\right)^n \frac{\cot\theta}{Re}, \tag{3.12}$$

where Re is the Reynolds number of the flow

$$Re \equiv \frac{\rho \bar{u}_0^{2-n} h_0^n}{\mu_n}. \tag{3.13}$$

Note that for a Newtonian fluid, $n = 1$, $Re = \rho \bar{u}_0 h_0/\mu_1$ is the customary Reynolds number. Equations (3.8) and (3.9) constitute the basic non-dimensional equations for $\bar{u}(x, t)$ and $h(x, t)$, with α and n as the parameters. For a given bed slope θ, the discharge $\langle Q \rangle$ and n may be regarded as the basic input; α and Re are derived parameters. From here on, unless stated otherwise, we shall use only dimensionless quantities and omit the asterisks for simplicity.

4. Linearized instability of uniform flow

Let a small perturbation be added to the uniform flow as follows:

$$h = 1 + H(x, t), \quad \bar{u} = 1 + \bar{U}(x, t), \tag{4.1}$$

where $H, U \ll 1$. Consider normal mode disturbances

$$(H, \bar{U}) = \mathrm{Re}\,(\hat{H}, \hat{U})\, e^{i(kx-\omega t)}, \tag{4.2}$$

where k is the real wavenumber, and $\omega = \omega_r + i\omega_i$ is complex. By standard linear analysis, an eigenvalue condition for non-trivial solutions of $\hat{H}$ and $\hat{U}$ is obtained:

$$\omega^2 - (2\beta k - in)\,\omega - i(1+2n)\,k + (\beta - \alpha)\,k^2 = 0, \tag{4.3}$$

which can be solved for ω:

$$\omega^{\pm} = \beta k - i\tfrac{1}{2}n \pm (a + ib)^{\frac{1}{2}}, \tag{4.4}$$

where

$$a = [\beta(\beta-1) + \alpha]\,k^2 - \tfrac{1}{4}n^2, \tag{4.5}$$

$$b = (1 + 2n - \beta n)\,k. \tag{4.6}$$

Since $0 < n \leqslant 1$, $0 < \beta \leqslant 1.2$, we must have $b > 0$ for $k \neq 0$. It follows that $a + ib$ lies in the upper complex plane, and the principal value of its square root must be in the first quadrant of the complex plane. Therefore

$$\omega_r^{\pm} = \beta k \pm \{\tfrac{1}{2}[a + (a^2 + b^2)^{\frac{1}{2}}]\}^{\frac{1}{2}}, \tag{4.7}$$

$$\omega_i^{\pm} = -\tfrac{1}{2}n \pm \{\tfrac{1}{2}[-a + (a^2 + b^2)^{\frac{1}{2}}]\}^{\frac{1}{2}} \tag{4.8}$$

Obviously $\omega_i^- < 0$; therefore ω^- corresponds to decay and stability. However ω_i^+ is negative if and only if

$$\{\tfrac{1}{2}[-a + (a^2 + b^2)^{\frac{1}{2}}]\}^{\frac{1}{2}} < \tfrac{1}{2}n, \tag{4.9}$$

which on substituting (4.5) and (4.6) is equivalent to

$$(1 + 2n - \beta n)^2 k^2 < n^2[\beta(\beta-1) + \alpha]\,k^2. \tag{4.10}$$

It follows that, for $k \neq 0$, disturbances will die out and the flow will be stable if

$$\alpha > \frac{1+2n}{n^2} \equiv \alpha_s(n) \quad \text{or} \quad Re < n\left(\frac{n}{1+2n}\right)^{1-n} \cot\theta. \tag{4.11}$$

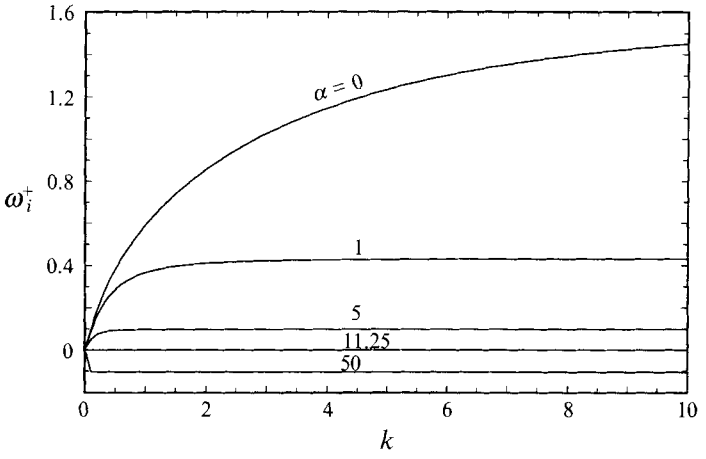

FIGURE 4. Growth rate of disturbance (ω_i^+) as a function of k and α for $n = 0.4$.

For a Newtonian fluid, the above instability criterion becomes

$$\alpha > 3 \quad \text{or} \quad Re < \cot\theta. \tag{4.12}$$

This has been obtained by Prokopiou *et al.* (1991) by using the Kármán momentum integral approximation with the parabolic profile ((2.9) with $n = 1$), also for $Re \gg 1$.

For low Reynolds numbers, $Re = O(1)$, and long waves, a rigorous result for the instability threshold is known from the solution of the Orr–Sommerfeld equation if the fluid is Newtonian (Benjamin 1957; Yih 1963). The result should also hold at high Re and serves as a check for the accuracy of the Kármán approximation. As shown by (B 17), the rigorous threshold for the Newtonian limit occurs at the slightly lower Reynolds number $Re = \frac{5}{6}\cot\theta$, recently verified experimentally by Liu *et al.* (1993). The numerical inaccuracy of (4.12) is due to the inaccuracy of the velocity profile associated with non-uniformity in the direction of flow, as pointed out already by Prokopiou *et al.* For power-law fluids we have carried out a rigorous instability analysis for $Re = O(1)$ and long waves, as given in Appendix B. It is shown that the approximate criterion (4.11) approaches the correct one (B 17) as n decreases, i.e. as the fluid becomes more shear thinning, suggesting that the Kármán approximation used here can be more reliable in the nonlinear problems studied here.

For general k the threshold of instability $\alpha_s(n)$ depends only on n. If $\alpha > \alpha_s$, all disturbances with $k \neq 0$ will be damped. The neutral stability curves are given by the two lines $k = 0$ and $\alpha = \alpha_s$. Figures 4 and 5 display, for $n = 0.4$, the monotonic dependence on k of the amplification rate ω_i^+ and the phase speed ω_r^+/k for various values of α. This monotonic tendency is expected to be altered by surface tension, which must be important for large k. For large k, the asymptotic amplification rate is

$$\omega_i^+ \sim -\frac{n}{2} + \frac{1+2n-\beta n}{2[\beta(\beta-1)+\alpha]^{\frac{1}{2}}} + \ldots, \tag{4.13}$$

while the phase speed is

$$\frac{\omega_r^+}{k} \sim \beta + [\beta(\beta-1)+\alpha]^{\frac{1}{2}} + \ldots. \tag{4.14}$$

Equation (4.14) has been used by Julien & Hartley (1985, 1986) to compare with the measured phase velocity of nonlinear laminar roll waves in water.

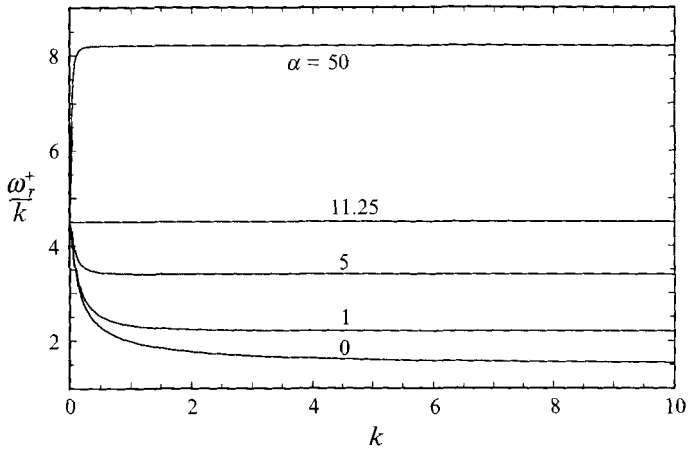

FIGURE 5. Phase speed of disturbance (ω_r^+/k) as a function of k and α for $n = 0.4$.

Note that at the long-wave limit, $k \sim 0$, the phase speed is given approximately by

$$\frac{\omega_r^+}{k} \sim \frac{1+2n}{n} + \ldots \quad (k \sim 0) \tag{4.15}$$

which depends on n only. In the Newtonian limit the phase speed is 3, as was also found by Prokopiou *et al.* (1991), and in agreement with the earlier theories for $Re = O(1)$ by Benjamin (1957) or Yih (1963).

5. Permanent roll wave

5.1. *The continuous profile between two shocks*

We consider roll waves in a permanent form moving at a constant speed c. Introducing a moving coordinate ξ given by

$$\xi = x - ct \tag{5.1}$$

and assuming that $\bar{u}$ and h are functions of ξ only, (3.8) can be integrated to

$$h(c-\bar{u}) = q, \tag{5.2}$$

where q is a constant which is the discharge rate as seen by an observer moving at the wave speed c. With (5.2), (3.9) gives the profile equation

$$\frac{\mathrm{d}h}{\mathrm{d}\xi} = \frac{h-(ch^{-1}-qh^{-2})^n}{(\beta-1)c^2-\beta q^2h^{-2}+\alpha h}\left(\equiv \frac{A(h)}{B(h)}\right), \tag{5.3}$$

where for subsequent discussions we denote the numerator and the denominator of (5.3) by $A(h)$ and $B(h)$ respectively. In accordance with all the reported observations, we seek a surface profile with its depth increasing monotonically towards the front, i.e. the slope $\mathrm{d}h/\mathrm{d}\xi > 0$ always. It follows that A and B must be of the same sign. It can be shown that for any $0 < n < 1$, the equation

$$A(h) = h - \left(\frac{c}{h} - \frac{q}{h^2}\right)^n = 0 \tag{5.4}$$

has one positive root when $q \leqslant 0$ and two or no positive roots when $q > 0$. It will be shown shortly by energy consideration that q must always be positive and therefore the

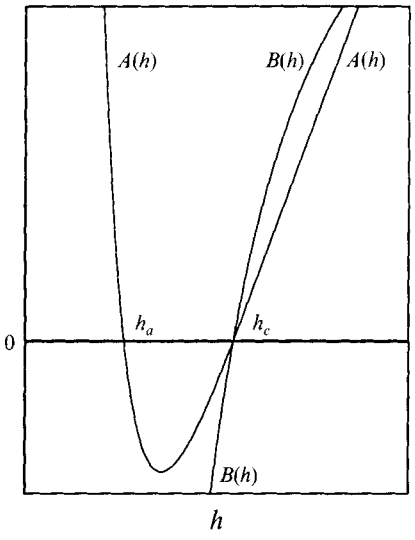

FIGURE 6. The numerator $A(h)$, and the denominator $B(h)$ of the profile equation as functions of h.

case of one positive root is impossible. Thus only the case of two positive roots is relevant to the present study. The two zeros of $A(h)$ will be denoted by h_a and h_c, where $h_a < h_c$, as shown in figure 6. On the other hand, $B(h)$ is monotonic in h with one zero, defined by

$$B(h) = (\beta - 1)\, c^2 - \frac{\beta q^2}{h^2} + \alpha h = 0, \tag{5.5}$$

as shown also in figure 6.

Note that $A'(h_a) < 0$, while $A'(h_c) > 0$. In order that the profile is continuous between two successive shocks and that $\mathrm{d}h/\mathrm{d}\xi > 0$, it is necessary that $B(h)$ also vanishes at h_c, which will be called the *critical depth*. The existence of the critical depth within the range (h_1, h_2) can be theoretically deduced, without assuming $\mathrm{d}h/\mathrm{d}\xi > 0$ in advance. This argument and physical discussions are given in Appendix C. The other root h_a must lie outside two successive shocks, and is an asymptote of the profile extended beyond the period.

Numerical integration of (5.3) will only give a smooth wave profile $h(\xi)$ monotonically increasing with ξ. For finite result it is necessary to match this profile with two shocks at the ends.

5.2. *The jump conditions and energy loss across a shock*

Referring to figure 7, we define λ to be the wavelength of the roll wave; $h_{1,2}$ the depth immediately before, after a shock; and $\langle h \rangle$ the average depth of the roll wave profile. By (5.3) we may write

$$\lambda = \xi(h_2) - \xi(h_1) = \int_{h_1}^{h_2} \frac{B(h)}{A(h)}\,\mathrm{d}h, \tag{5.6}$$

$$\langle h \rangle = \lambda^{-1} \int_0^{\lambda} h\,\mathrm{d}\xi = \lambda^{-1} \int_{h_1}^{h_2} \frac{hB(h)}{A(h)}\,\mathrm{d}h. \tag{5.7}$$

It is clear that

$$h_a < h_1 < \langle h \rangle < h_2. \tag{5.8}$$

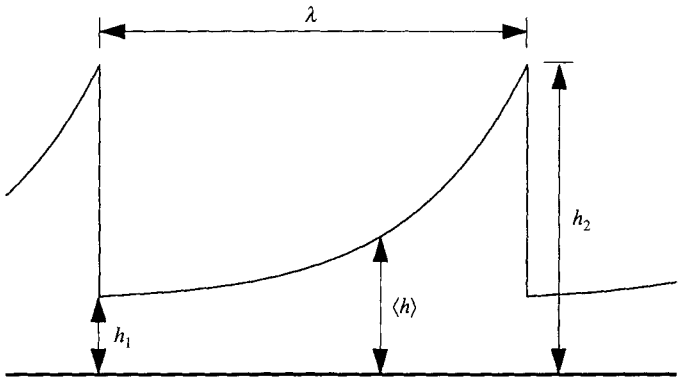

FIGURE 7. Definition sketch of a roll wave profile.

Note that in general $\langle h\rangle \neq 1$. The average discharge rate $\langle Q\rangle$ defined by (3.1), together with (5.2) and the definition of $\langle h\rangle$, implies another relation:

$$1 = c\langle h\rangle - q \tag{5.9}$$

since the normalized $\langle Q\rangle$ is 1 by (3.4) and (3.7*b*). Though roll waves are not sinusoidal, we may still define the wavenumber according to

$$k = 2\pi/\lambda. \tag{5.10}$$

The shock conditions are derived from the conservation laws of mass and momentum† in (3.8) and (3.9):

$$c[h]_1^2 = [\bar{u}h]_1^2, \tag{5.11}$$

$$c[\bar{u}h]_1^2 = [\beta\bar{u}^2h + \tfrac{1}{2}\alpha h^2]_1^2, \tag{5.12}$$

where $[h]_1^2 \equiv h_2 - h_1$, etc. After eliminating $\bar{u}$ from (5.12), we get a relation between the two depths h_1 and h_2:

$$\alpha h_1 h_2^2 + \alpha h_1^2 h_2 + 2(\beta-1)c^2 h_1 h_2 - 2\beta q^2 = 0, \tag{5.13}$$

which can be solved for h_2:

$$h_2 = -\left[\frac{h_1}{2} + (\beta-1)\frac{c^2}{\alpha}\right] + \left\{\left[\frac{h_1}{2} + (\beta-1)\frac{c^2}{\alpha}\right]^2 + \frac{2\beta q^2}{\alpha h_1}\right\}^{\frac{1}{2}} \tag{5.14a}$$

for $\alpha > 0$, and

$$h_2 = \frac{\beta q^2}{(\beta-1)c^2 h_1} \tag{5.14b}$$

for $\alpha = 0$ (vertical wall).

It is well-known that across a hydraulic jump in conventional open channels some of the mechanical energy is lost through turbulence to heat. By considering a small control volume which just encloses the shock and moves at the same speed c, the rate of change of mechanical energy across the jump can be found, in physical quantities,

$$\dot{E} = \left[\int_0^h \{(\tfrac{1}{2}\rho u^2 + \rho g\cos\theta z)(u-c) + pu\}\,\mathrm{d}z\right]_2^1. \tag{5.15}$$

† In hyperbolic systems these physical laws can often be manipulated so that they are written in mathematically different conservation forms. However, the conservation laws appropriate for shock conditions must be consistent with the integral conservation laws of the physics in the present case (Whitham 1974, p. 41).

With the pressure given by (2.7), the integration can be formally carried out for any velocity profile:

$$\dot{E} = [\tfrac{1}{2}\gamma\rho\bar{u}^3 h - \tfrac{1}{2}\beta\rho c\bar{u}^2 h - \tfrac{1}{2}\rho g\cos\theta ch^2 + \rho g\cos\theta\bar{u}h^2]_2^1, \tag{5.16}$$

where γ is the energy flux factor

$$\gamma \equiv (\bar{u}^3 h)^{-1}\int_0^h u^3\,\mathrm{d}z. \tag{5.17}$$

Making use of (5.2) and (5.13), we obtain a normalized relation

$$\dot{E}^* \equiv \frac{\dot{E}}{\rho\bar{u}_0^3 h_0} = (h_2^*-h_1^*)\left[-q^*\left\{\frac{\gamma}{4\beta}\alpha\frac{(h_2^*-h_1^*)^2}{h_2^* h_1^*}+\frac{\gamma-\beta}{\beta}\alpha+\frac{\gamma(\beta-1)}{2\beta}c^{*2}\frac{h_2^*+h_1^*}{h_2^* h_1^*}\right\}\right.$$
$$\left.+\frac{3(\gamma-\beta)}{4\beta}\alpha c^*(h_2^*+h_1^*)+\frac{2\gamma\beta-3\gamma+\beta}{2\beta}c^{*3}\right]. \tag{5.18}$$

If the velocity profile were to be uniform, the flux factors β and γ would be equal to unity, then

$$\dot{E}^* = -q^*\alpha\frac{(h_2^*-h_1^*)^3}{4h_2^* h_1^*}. \tag{5.19}$$

Thus for uniform profiles, $\dot{E}^*$ is negative as long as $h_2^* > h_1^*$ and $q_* > 0$, and $\dot{E}^* = 0$ only when $h_1^* = h_2^*$. However, it is physically unrealistic and inconsistent to use a uniform profile near the shock in a laminar flow.† For any non-uniform profile in general, the two flux factors are different and (5.19) is no longer true. For general profiles, if the flux factors satisfy

$$\beta > 1, \quad \gamma-\beta > 0 \quad \text{and} \quad 2\gamma\beta-3\gamma+\beta > 0 \tag{5.20}$$

a necessary condition for $\dot{E} < 0$ is

$$q > q_c \equiv \left[\frac{3(\gamma-\beta)}{4\beta}\alpha c(h_2+h_1)+\frac{2\gamma\beta-3\gamma+\beta}{2\beta}c^3\right]$$
$$\times\left\{\frac{\gamma}{4\beta}\alpha\frac{(h_2-h_1)^2}{h_2 h_1}+\frac{\gamma-\beta}{\beta}\alpha+\frac{\gamma(\beta-1)}{2\beta}c^2\frac{h_2+h_1}{h_2 h_1}\right\}^{-1} > 0, \tag{5.21}$$

where we have dropped the asterisks. In particular for the assumed profile (2.9), β is given by (2.16) and

$$\gamma = \frac{6(1+2n)^2}{(2+3n)(3+4n)}. \tag{5.22}$$

It can easily be proved that the conditions (5.20) are satisfied. Substituting γ and β into (5.21), we get

$$q_c = \left[\frac{3n}{2(3+4n)}\alpha c(h_2+h_1)+\frac{(1+3n)n}{(2+3n)(3+4n)}c^3\right]$$
$$\times\left\{\frac{3(1+2n)}{4(3+4n)}\alpha\frac{(h_2-h_1)^2}{h_2 h_1}+\frac{2n}{3+4n}\alpha+\frac{3(1+2n)n}{2(2+3n)(3+4n)}c^2\frac{h_2+h_1}{h_2 h_1}\right\}^{-1}. \tag{5.23}$$

† For roll waves in a Newtonian layer, Ishihara *et al.* (1954) assumed a parabolic profile away from the shock but uniform profiles near the shock. This is of course inconsistent.

Thus for laminar flow there is a minimum discharge in the moving coordinate system below which stationary roll waves cannot be maintained. Since q must also be positive, it follows from (5.2) that the shock speed c must be greater than the speed of the fluid particles. At the lower limit $q = q_c$, $\dot{E} = 0$, i.e. there is no loss of energy across the shock but the shock amplitude is finite. In principle an exact theory involving derivatives of all orders and surface tension is needed near the shock, so that shocks are only approximations to steep and continuous fronts.

5.3. *Procedure of numerical solution*

In principle we may specify three parameters: n, α, λ (or k) in order to solve for the other variables: c, q, h_c, $\langle h\rangle$, h_1, h_2 from equations (5.6), (5.7), (5.9), (5.14), (5.4) and (5.5). To generate results for all possible λ, it is more convenient to specify h_c and find λ instead. After completing the solution, the rate of energy dissipation across the shock is calculated according to (5.18) in order to rule out physically unacceptable solutions. The numerical procedure is as follows:

(i) for given n, α, choose h_c;

(ii) solve for q and c from (5.4) and (5.5)

$$q = (\beta-1)\,h_c^{\frac{1+2n}{n}} + [\beta(\beta-1)\,h_c^{\frac{2(1+2n)}{n}} + \alpha h_c^3]^{\frac{1}{2}}, \tag{5.24}$$

$$c = h_c^{\frac{1+n}{n}} + q h_c^{-1}; \tag{5.25}$$

(iii) find $\langle h\rangle$ from (5.9)

$$\langle h\rangle = \frac{1+q}{c}; \tag{5.26}$$

(iv) find λ, h_1 and h_2 from (5.6), (5.7) and (5.14):

$$\langle h\rangle\,\lambda = \int_{h_1}^{h_2(h_1)} \frac{hB(h)}{A(h)}\,\mathrm{d}h, \tag{5.27}$$

where

$$\lambda = \int_{h_1}^{h_2(h_1)} \frac{B(h)}{A(h)}\,\mathrm{d}h. \tag{5.28}$$

5.4. *Admissible range of* α

The energy condition (5.21) contains h_1 and h_2 which are not known until the last step of the solution process, and therefore in general gives no clue in advance about the acceptable ranges of the parameters. We now explore two conditions with a view to forecasting, for a given n, the admissible range of α and the corresponding range of h_c.

Recall first that $A'(h_c) > 0$. By differentiating $A(h)$, we get

$$1 + n h_c^{\frac{n-1}{n}} [h_c^{\frac{1-n}{n}} - q h_c^{-3}] > 0 \tag{5.29}$$

which can be simplified as

$$\left(\frac{1+n}{n}\right) h_c^{\frac{1+2n}{n}} > q. \tag{5.30}$$

By inserting the relation (5.24) between q and h_c we obtain the first condition for α:

$$G(h_c) \equiv \left(\frac{1+2n}{n^2}\right) h_c^{\frac{2+n}{n}} > \alpha. \tag{5.31}$$

We prove in Appendix D that h_a, $\langle h\rangle$, 1, and h_c are in generall all different, and

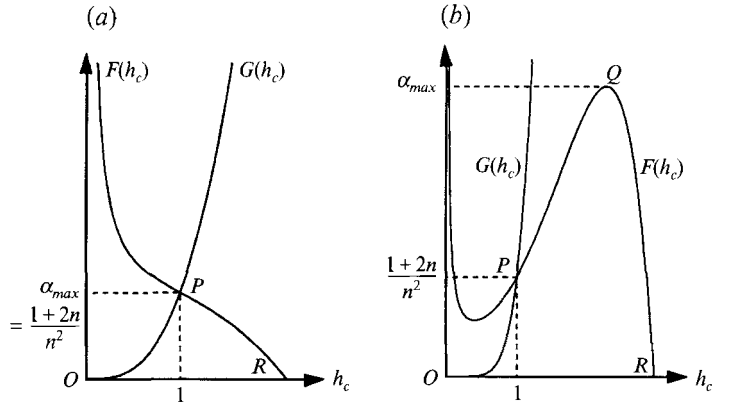

FIGURE 8. The functions $F(h_c)$ and $G(h_c)$: (a) $n \geqslant 1/\sqrt{2}$, (b) $n < 1/\sqrt{2}$; $F(h_c) = \alpha$ corresponds to a solitary bore.

$h = 1$ must always lie between $\langle h \rangle$ and h_c. From figure 6, it is evident that, since $h_a < 1$,

$$A(1)\begin{cases} < 0 & \text{if} \quad h_c > 1; \\ > 0 & \text{if} \quad h_c < 1. \end{cases}$$

Since $A(1) = 1-(c-q)^n$ we have

$$c\begin{cases} > 1+q & \text{if} \quad h_c > 1; \\ < 1+q & \text{if} \quad h_c < 1. \end{cases}$$

Because of (5.25), both inequalities imply

$$\frac{h_c^{\frac{1+2n}{n}} - h_c}{h_c - 1} > q. \tag{5.32}$$

With the help of (5.24), (5.32) can be written as

$$\frac{-(\beta-1)h_c^{\frac{1+3n}{n}} + \beta h_c^{\frac{1+2n}{n}} - h_c}{h_c - 1} > [\beta(\beta-1)h_c^{\frac{2(1+2n)}{n}} + \alpha h_c^3]^{\frac{1}{2}}. \tag{5.33}$$

Squaring both sides of (5.33), we finally obtain a second condition for α:

$$F(h_c) \equiv \frac{-(\beta-1)h_c^{\frac{2(1+2n)}{n}} + \beta h_c^{\frac{2(1+n)}{n}} + 2(\beta-1)h_c^{\frac{1+2n}{n}} - 2\beta h_c^{\frac{1+n}{n}} + 1}{(h_c-1)^2 h_c} > \alpha. \tag{5.34}$$

The two functions $F(h_c)$ and $G(h_c)$ are plotted in figure 8. We emphasize that (5.31) and (5.34) are necessary, but not sufficient, conditions for the existence of an acceptable roll wave solution. All final results must still be scrutinized by the energy condition (5.21).

Let us examine the properties of these functions and their implications:

(i) For all n, $G(h_c)$ is a monotonically increasing function of h_c.

(ii) At $h_c = 1$, F and G are equal:

$$G(1) = F(1) = \frac{1+2n}{n^2} = \alpha_s(n), \tag{5.35}$$

which is the stability limit of infinitesimal disturbances on a uniform flow of depth 1.

(iii) $F(h_c)$ is a monotonically decreasing function when $1 > n \geqslant 1/\sqrt{2}$ (figure 8*a*), i.e. for a slightly non-Newtonian fluid. However, for $0 < n < 1/\sqrt{2}$, i.e. highly non-Newtonian fluid, the curve exhibits two extrema and concaves upward for $h_c < 1$ but downward for $h_c > 1$ (figure 8*b*). The critical value $n = 1/\sqrt{2}$ is obtained by equating $F'(h_c)$ at $h_c = 1$ to zero,

$$\lim_{h_c \to 1} F'(h_c) = -\frac{(2n^2-1)(1+2n)(2+n)}{n^3(2+3n)} = 0. \tag{5.36}$$

Now we separate two cases: $h_c > 1$ and $h_c < 1$.

(iv) For $h_c > 1$, $G(h_c) > F(h_c)$ for all values of n.

(v) According to (5.31) and (5.34), a solution exists for an h_c only if α is less than both $F(h_c)$ and $G(h_c)$, i.e. under the curves OPR and $OPQR$ respectively in figures 8(*a*) and 8(*b*). Note that for $n \geqslant 1/\sqrt{2}$ no roll wave will exist if $\alpha > \alpha_s$, i.e. if the uniform flow is stable to infinitesimal disturbances. However for $n < 1/\sqrt{2}$, the local maximum of $F(h_c)$ (Q in figure 8*b*) which can be found numerically, is greater than α_s. This implies that for $n < 1/\sqrt{2}$, there exists roll wave solution even then the corresponding uniform flow is stable! This contrasts sharply with the result of Dressler & Pohle (1953) who found that, in clear water open-channel flows, no roll wave solutions exist when the uniform flow is linearly stable.

(iv) When $G(h_c) = \alpha$ and $h_c < 1$ (on OP in figure 8*a*, *b*), we have $A'(h_c) = 0$, which implies $h_c = h_a$. Since h_1 must be between h_c and h_a, the case corresponds to the limit that h_2, $\langle h \rangle$, h_c, h_1, and h_a collapse to one value which is less than unity. Obviously this is physically impossible and therefore no solutions will exist along OP.

(vii) When $h_c = 1$ and $\alpha \leqslant \alpha_s$ (on $P1$ in figure 8*a*, *b*), we have $\langle h \rangle = h_c = 1$. This case can be studied by perturbing h_c to $1+\varepsilon$ where $\varepsilon \ll 1$. Though the details are omitted here, the analysis indicates that as $\varepsilon \to 0$, the two depths $h_{2,1} \to 1 \pm O(\delta)$ where $O(\varepsilon) \leqslant \delta \ll 1$. Therefore the wave height is of order δ which is very small. Putting these limiting values into the energy relation (5.21), we find that as $h_c \to 1$

$$\dot{E} \to O(\delta)\frac{n}{3+4n}[-q\{2\alpha+\tfrac{3}{2}\beta c^2\}+3\alpha c+\tfrac{1}{2}\beta c^3]. \tag{5.37}$$

Using the limiting values of q and c given by (5.24) and (5.25)

$$q \to \beta - 1 + [\beta(\beta-1)+\alpha]^{\frac{1}{2}},$$
$$c \to 1+q,$$

and the maximum α being $(1+2n)/n^2$, we can prove that the terms inside the square brackets in (5.37) always end up with a positive sum. Therefore, when the computed wave height is small compared with the mean flow depth, the energy requirement is always violated and no physical roll waves will exist.

(viii) When $F(h_c) = \alpha$ and $h_c > 1$ (on PR in figure 8*a* or PQR in figure 8*b*), we have $A(1) = 0$ which implies $h_a = 1$ (since $A(h) = 0$ has only two positive roots and now $h_c > 1$). As $h = 1$ is always a section in a profile and $\langle h \rangle$ is now less than 1 in accordance with (D 3), we must conclude that

$$h_a \to h_1 \to \langle h \rangle \to 1 < h_c < h_2. \tag{5.38}$$

Because of (5.6), the wave must be infinitely long ($\lambda = \infty$), and may be called a *solitary* roll wave. Furthermore for $n < 1/\sqrt{2}$ and $\alpha_{max} > \alpha > \alpha_s$, there are two h_c values satisfying $F(h_c) = \alpha$ and therefore two *solitary* waves are possible. Variations of α_{max} and α_s with n are shown in figure 9.

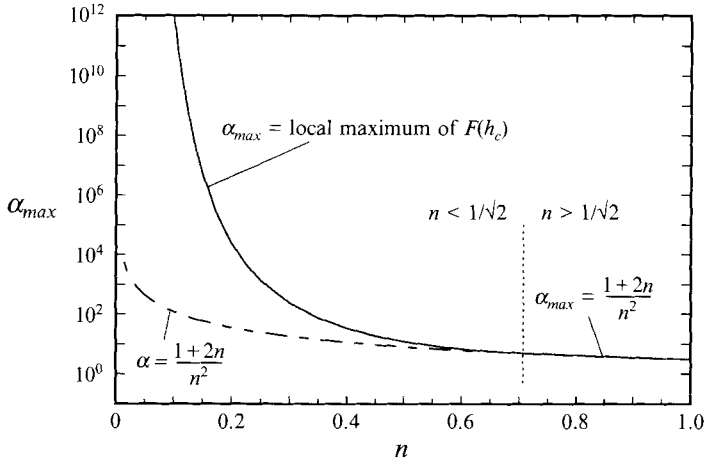

FIGURE 9. Relation of α_{max} with n.

6. Numerical results

As a basis for comparison, the Newtonian case $n = 1.0$ is examined first and checked against experiments. Two non-Newtonian fluids with $n = 0.4$ and 0.1 have been studied; the results for $n = 0.4$ are representative and will be discussed.

6.1. *A Newtonian layer*

When $n = 1$, the maximum allowable $\alpha_s(1)$ is 3. Computations have been carried out for $\alpha = 0$, 0.25, 0.5, and 1, all less than $\alpha_s = 3$. In figure 10, solid lines represent the dimensionless wave speed c *vs.* the dimensionless wavenumber k. Also plotted as the long-dashed line is the threshold $q = q_c$ corresponding to zero energy dissipation across the shock. Roll waves exist only when $k < k_c$ and when $c > c_c$ where k_c and c_c are the corresponding thresholds. For larger α, k_c is smaller but c_c is greater. In figure 11, we show the dependence of the dimensionless wave height $H = h_2 - h_1$ on the dimensionless wavenumber k. Again, the thresholds are joined by a dashed line. For all values, the threshold H_c is the minimum possible wave height and is smaller for larger α.

In figure 10, we also show as short dashes the dispersion relation between c and k for an infinitesimal wave according to the linearized theory (4.4). Clearly the linear and nonlinear theories are closest for the higher range $k \leqslant k_c$ where the roll wave height H_c is smallest. For smaller k, the departure is more pronounced, showing the inadequacy of linearization. At the limit $k = 0$, curves of the linearized theory converge to $c = 3$, which can be calculated from (4.16), while those of the roll waves rise up drastically to much higher values of c. For clarity these limiting values of c for solitary roll waves are plotted against α in the smaller graph inserted in figure 10. Similarly, H also increases sharply at the limit $k = 0$, as shown in the insert to figure 11. Note that for a given α, the solitary roll wave has the greatest c and H.

Recall from the linearized theory that the growth rate of unstable infinitesimal disturbances increases monotonically with k (figure 4). Thus the shorter the disturbance, the more likely it will reach the nonlinear state of roll waves. However, there is no finite wavenumber which has the largest growth rate; therefore, the linear analysis alone is insufficient to forecast the likely wavelength of the nonlinear roll waves. On the other hand, nonlinear roll waves can exist only when k is below the threshold k_c, otherwise the results would imply energy gain across the shock and be unphysical. We now propose that roll waves generated spontaneously from linearized

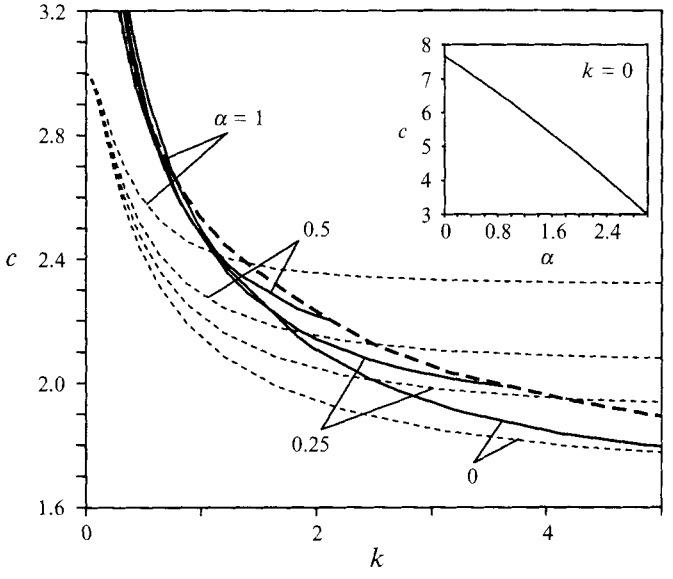

FIGURE 10. c as a function of k and α for $n = 1.0$: ——, roll wave theory; — — — —, $q = q_c$; – – –, linear theory. (Insert: c *vs.* α for $k = 0$.)

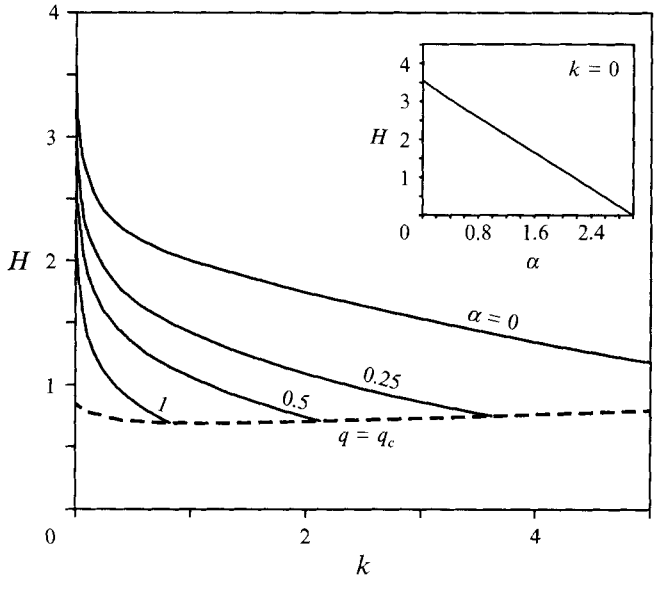

FIGURE 11. H as a function of k and α for $n = 1.0$. (Insert: H *vs.* α for $k = 0$.)

disturbances should have the fastest initial growth and at the same time satisfy the nonlinear constraint that energy is not created across a shock. To meet both requirements the preferred wavenumber of such a roll wave is simply k_c, corresponding to the shortest wavelength $\lambda_c = 2\pi/k_c$, the smallest wave speed c_c and height H_c, and no energy loss at the jump. We shall call this the *minimum roll wave*. This criterion is not far from that of Kapitza (1948) who suggested that the wave with the smallest mean energy (averaged over the wavelength) is the observed one. At the shock, the gradient is of course too large so that the long-wave approximation must require local

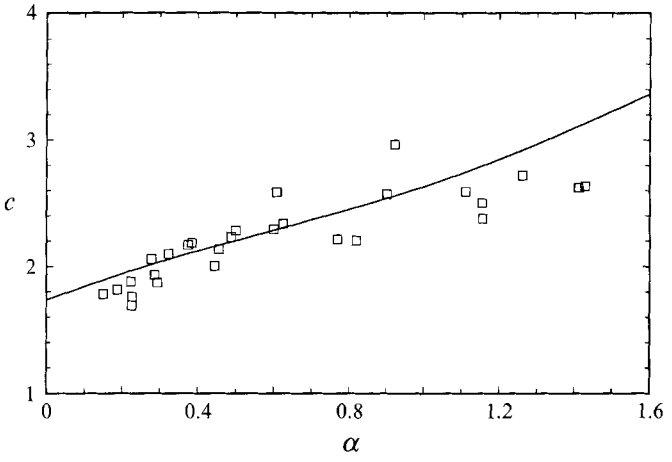

FIGURE 12. Comparison of the minimum roll wave c *vs.* α for $n = 1.0$ (——) with experimental data from Julien & Hartley (1985), □.

improvement, such as higher orders and surface tension. Indeed some of Kapitza's photographs have shown a sequence of step fronts with weakly rippled tails, which may be regarded as the more accurate picture of roll waves described here. (See Prokopiou *et al.* 1991 for theory of these waves and Liu *et al.* 1993 for further experiments.)

Roll waves of longer wavelengths, corresponding to positive dissipation across the shock can still be generated, of course, by imposing initial or boundary conditions, for example by periodically varying the influx rate at far upstream at different periods where infinitesimal disturbances are unstable.

Experiments on roll waves on a thin laminar layer of water have been reported by Ishihara *et al.* (1954), Mayer (1959), and Julien & Hartley (1985). Ishihara *et al.* (1954) carried out tests in a channel 6 m long, 0.2 m wide and maximum slope $\sin\theta = 0.2$. The range of Re is 50–500, and the water depths are from 1 to several millimeters. They observed no roll waves when $\alpha > 1.2$. The profiles of the laminar wave front was not steep but was smooth and with a round crest. Mayer (1959) conducted tests in a channel 8 m long and 0.5 m wide. Laminar roll waves were observed for $80 < Re < 420$ and at a channel slope between 0.035 and 0.088. Near the upstream end the incipient roll waves were formed after the surface irregularities had coalesced and become ridges which then tended to steepen in the front and flatten at the back. Further downstream the roll wave would continue to grow in height, speed and wavelength. Mayer however did not present any numerical data relating the wavelengths with Re or the speeds. He noticed that only those waves with a short formation length would attain a terminal status before exiting the channel.

The most comprehensive report for spontaneously developed roll waves in laminar flow of water is by Julien & Hartley (1985) who used a relatively long channel of 9.75 m in length and 0.21 m in width. They determined the wave period by counting the number of waves over a time interval at the downstream exit. The wave velocity was determined by taking the time intervals of several wave crests to travel a distance of 1.52 m and then averaging the results. The range of Re is between 65 and 550 and the slope between 0.015 and 0.04, the water depths were in the order of millimeters. A numerical summary of the wave velocity, period, the slope and Re was given.

In all these experiments on roll wave on laminar films, details of the wave front have never been fully and consistently described. Surface tension may contribute to the

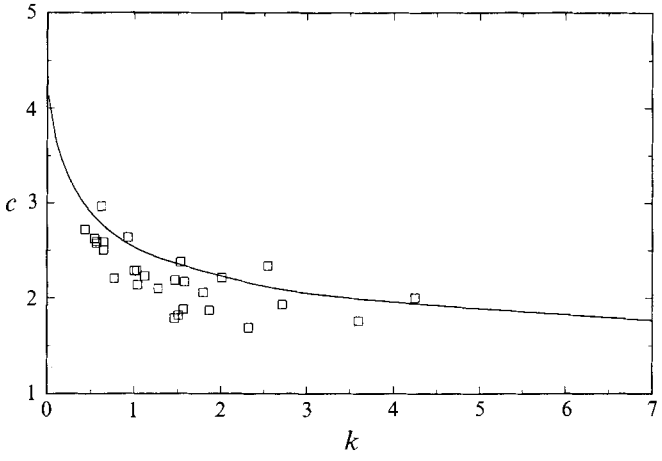

FIGURE 13. Comparison of the minimum roll wave k *vs.* c for $n = 1.0$ (——) with experimental data from Julien & Hartley (1985), □.

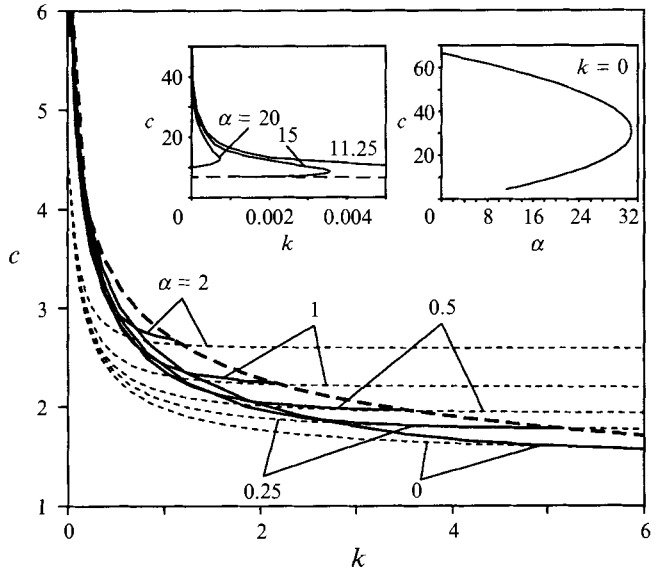

FIGURE 14. c as a function of k and α for $n = 0.4$: ——, roll wave theory; ———, $q = q_c$; – – – –, linear theory. (Left insert: enlarged plot for small k; right insert: c *vs.* α for $k = 0$.)

roundedness at the wave front. With these reservations we compare our minimum roll wave theory with the measurements of Julien & Hartley in figure 12 for α *vs.* c, and figure 13 for the dispersion curve c *vs.* k. All data points scatter around the theoretical curves for minimum roll waves, suggesting that the combination of criteria based on linearized instability and energy consideration is a reasonable approach for determining the wavelength of roll waves developed spontaneously from unstable infinitesimal waves.

6.2. *Non-Newtonian roll waves*

We only present results for $n = 0.4 < 1/\sqrt{2}$. The upper limit of stability for linearized disturbances is $\alpha_s = 11.25$ while the maximum allowable α, α_{max}, for the existence of roll waves is 32 (figure 9). In figures 14 and 15, we plot c and H against k respectively,

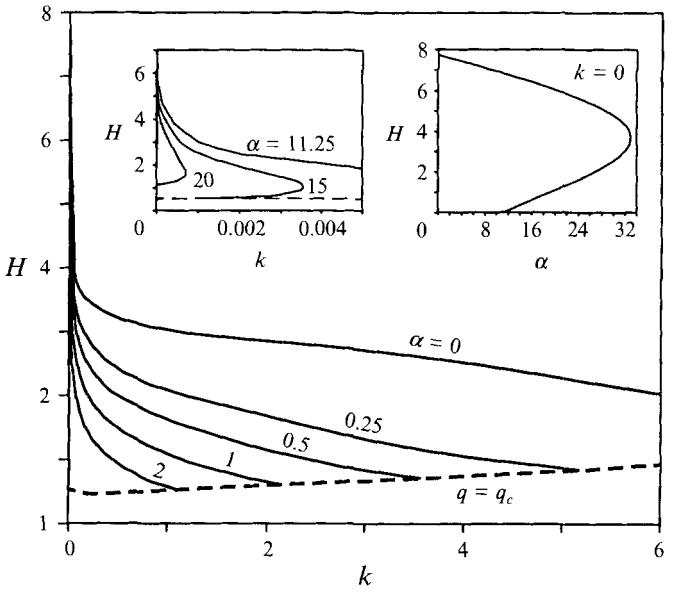

FIGURE 15. H as a function of k and α for $n = 0.4$. (Left insert: enlarged plot for small k; right insert: H *vs.* α for $k = 0$.)

with $\alpha = 0$, 0.25, 0.5, 1, 2, 11.25, 15 and 20. The basic features of the two graphs resemble their counterparts in the Newtonian case. A dashed line is drawn in each plot to indicate the threshold $q = q_c$; solutions to the right of the threshold have been discarded by the energy criterion (5.21). Results of the linearized theory are also shown in figure 14 for comparison to the roll wave solutions. For small enough k the height H of the roll wave increases and the speeds given by the two theories diverge. The speeds and the heights of the infinitely long, or solitary, roll waves are shown in the insert. The solitary roll waves here have rather high speeds and heights. For such large amplitudes, the local Reynolds number near the wave crest is greater than the limiting Reynolds number for laminar flow; the calculated results for this case are therefore unreliable. For example, when $\alpha = 0.25$, the solitary wave has the normalized $h_2 = 8.7$ and $\bar{u}_2 = 58.9$. If the slope $\theta = 0.1$ rad. the Reynolds number of the uniform flow is, by (3.12), 73. Then by (3.13) the local Reynolds number at the crest is

$$58.9^{1.6} \times 8.7^{0.4} \times 73 = O(1 \times 10^5)$$

which must be in the turbulent regime, as the upper bound for a laminar flow of $n = 0.4$ is only $R_c = 492$ (§3).

An interesting difference between the non-Newtonian and Newtonian theories is the existence of roll waves when α is equal to or greater than α_s, which is the upper limit of instability, provided that $n < 1/\sqrt{2}$. Recall that according to the linearized theory, all infinitesimal waves are damped out if $\alpha > \alpha_s$. These solutions can be double-valued, as suggested by figure 8(*b*). The results are now shown in figures 14 and 15, for $\alpha = 11.25$, 15 and 20. There are two solutions for each k when $\alpha < \alpha_s = 11.25$. For any α there is a maximum k_{max}. Therefore there are two solutions for any k between the threshold k_c and the maximum k_{max}. However, for small enough α only one satisfies the energy criterion. For $\alpha = 20$, both branches have admissible solutions at $k = 0$ and therefore two solitary roll waves, each with different speed and height. Numerically we find two solitary waves for any α between 18 and 32. The upper and the lower branches

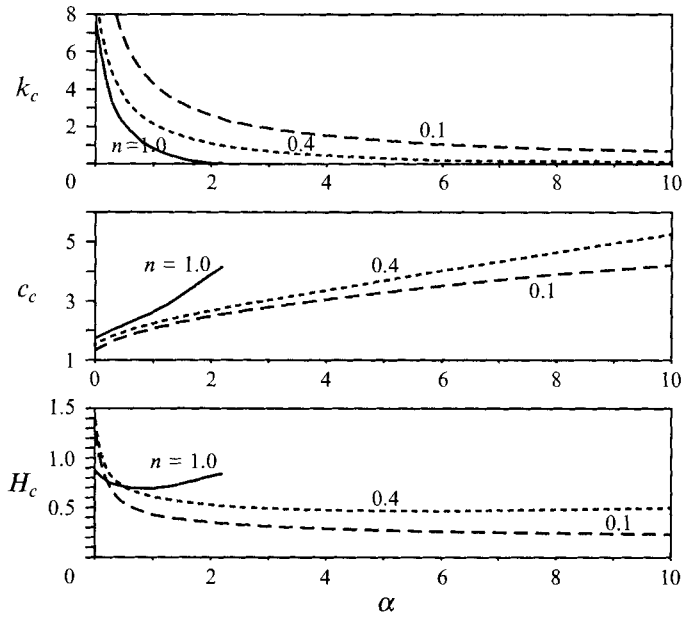

FIGURE 16. Minimum roll wave relations between k_c, c_c, H_c and α for $n = 1.0$, 0.4, 0.1.

give respectively higher and smaller values of speed and height for the solitary waves. The two branches meet at $\alpha_{max} = 32$. Again, whether these solitary waves are physically possible depends on whether the flow is still laminar. This depends on the bed slope which in turn determines the Reynolds number of the uniform flow.

6.3. *The minimum roll wave*

So far no experiments are known for spontaneously generated roll waves in power-law fluids. We present here the calculated threshold relations for the non-Newtonian cases $n = 0.4$ and 0.1 in figure 16, in which the results for a Newtonian fluid ($n = 1$) are also included for comparison. It can be seen that for each n, k decreases and c increases when α increases under the present normalization. The wave height H drops first and then increases as α increases. Recall that for the Newtonian case $\alpha_{max} = \alpha_s = 3$, but the maximum α that yields solutions satisfying the energy criterion is only slightly above 2.

6.4. *Roll wave profiles*

Sample profiles of the free surface $h(\xi)$, the mean fluid velocity $\bar{u}(\xi)$ and the bottom stress $\tau_b(\xi)$ will now be presented. The velocity is computed from (5.2), and the bottom stress from (3.10). Recall from definitions that a decrease in α reflects an increase in either the flow rate or the slope. For a fixed slope, an increase in discharge will increase the scales for the depth, the longitudinal length, velocity and the bottom stress. For a fixed discharge, an increase in the slope will result in a decrease in the scales for the depth, but an increase in the scales for the longitudinal length (except when $n = 1$), velocity and the bottom stress.

First we consider the minimum roll waves. In figure 17, we show the profiles for $h(\xi)$, $\bar{u}(\xi)$ and $\tau_b(\xi)$ for $k = k_c$ and $\alpha = 0$, 1 and 5 for $n = 0.4$. Note that the three α values represent respectively a vertical wall and two planes of mild slopes. For example, if the Reynolds number of the uniform flow is 100, the slope is given by (3.12), $\tan\theta = 4.5^{0.4}/100\alpha$, then $\theta = \frac{1}{2}\pi$, 0.018, and 3.7×10^{-3} rad respectively for the above

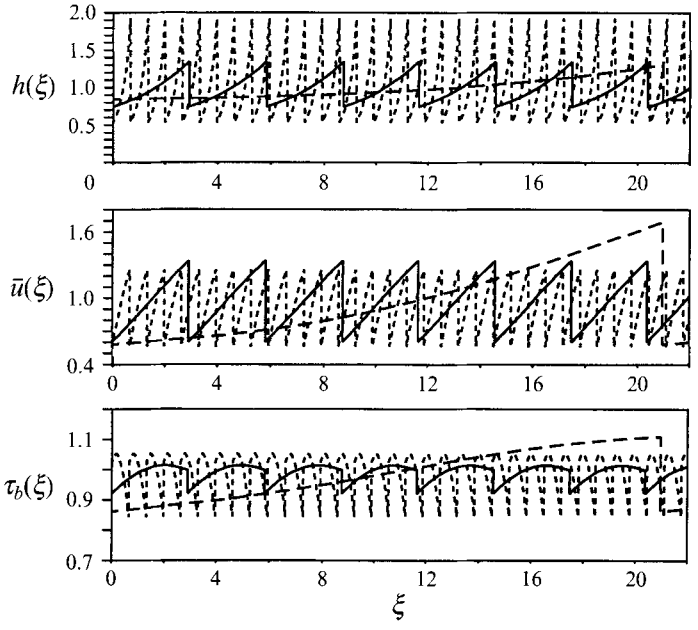

FIGURE 17. Profiles for minimum roll waves $k = k_c$ for $n = 0.4$, and $\alpha = 0$ (– – – –), 1 (——), 5 (— — —).

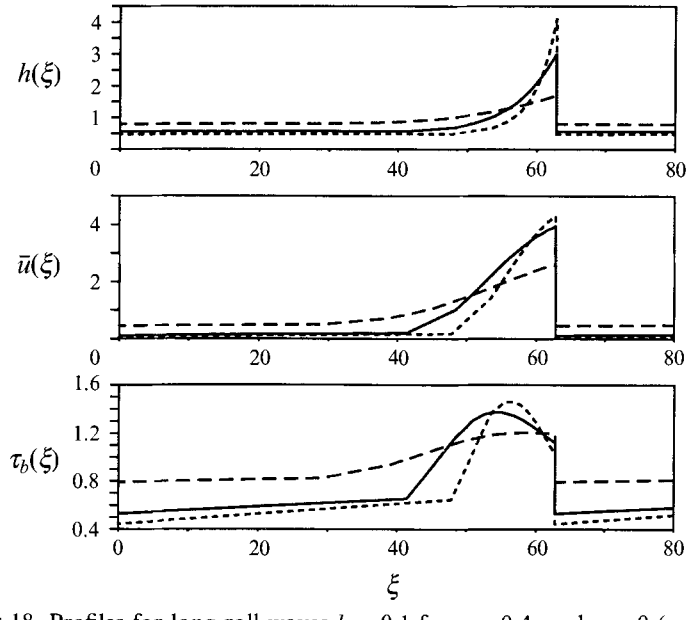

FIGURE 18. Profiles for long roll waves $k = 0.1$ for $n = 0.4$, and $\alpha = 0$ (– – – –), 1 (——), 5 (— — —).

three α values. From figure 17, we observe that $\alpha = 0$ gives the highest and the shortest roll wave where the maximum depth is almost twice that of the uniform flow depth. The peak fluid speed is about 30% higher than the uniform flow speed. As α increases, slope decreases, the normalized wave length increases and the normalized amplitude decreases. It is also clear that the peak bottom stresses exceed the uniform flow value by only a modest amount (the maximum being 10% for $\alpha = 5$). Similar results have

also been obtained for $n = 1$ (Newtonian) and $n = 0.1$ (highly non-Newtonian). In general, the flow depth and velocity in these roll waves differ considerably from the corresponding uniform flow, but the bottom stress remains much the same. Spatially the maximum of τ_b occurs near the middle of a period for $\alpha = 0$, but shifts towards the front with larger α.

We next consider much longer waves for $n = 0.4$ for the same three values of $\alpha = 0, 1, 5$. Though the solitary wave ($k = 0$) is the strongest theoretically, we avoid the extreme case of high speeds and amplitude and consider $k = 0.1$, as shown in figure 18. The highest wave is given by $\alpha = 0$ (vertical wall). From the velocity profiles the flow is seen to have practically vanished when the depth is below a certain value. As a result, the fluid appears stagnant along more than half of the stretch in the rear of the period, while moving with a tremendous speed in the front half. This behaviour closely resembles the bursting mud flows characterized by a period of cessation of flow between successive waves, as described by Li *et al.* (1983). These long roll waves are potentially more damaging than the minimum roll waves and the corresponding uniform flows.

7. Conclusions

Based on the long-wave approximation, a theory of roll waves has been developed for non-Newtonian mud flows whose rheological behaviour is modelled by a power law. For a fluid of flow index above $1/\sqrt{2}$, there exists no roll wave solutions if the corresponding uniform flow is stable according to the linear theory. However for $n < 1/\sqrt{2}$, i.e. highly non-Newtonian, it is possible for very long waves with large amplitudes to exist even when the corresponding uniform flow is stable. An energy criterion is introduced to predict the wavelength of the roll wave spontaneously developed from unstable infinitesimal disturbances. Such a roll wave has the shortest wavelength and lowest amplitude without energy loss across the shock. In the Newtonian limit the properties of the minimum roll wave appear to be consistent with the available experimental data for a thin sheet of water. In the non-Newtonian cases these roll waves have appreciably different velocities and depth profiles, but nearly the same bottom stress as the uniform flows with the same discharge. However, for longer roll waves the kinematics and dynamics of the flow at the front can be much more vigorous than those far behind the front. This is consistent with the field observations of bursts, which pose much greater threats in bottom scour.

We thank the US Office of Naval Research, Ocean Engineering Division (Contract N00014-89-J-3128) and National Science Foundation, Natural Hazards Program (Grant BCS-9112748) for supporting this research.

Appendix A. Equations of motion for the long-wave approximation

We wish to show the conditions under which (2.1)–(2.7) are valid. For the power-law fluid, we introduce the following normalizations into the full Navier–Stokes equations:

$$x = l_0 x^*, \quad z = h_0 z^*, \quad p = \rho \bar{u}_0^2 p^*, \tag{A 1a}$$

$$u = \bar{u}_0 u^*, \quad v = \bar{u}_0 (h_0/l_0)\, v^*, \quad t = (l_0/\bar{u}_0)\, t^*, \tag{A 1b}$$

$$(\tau_{xx}, \tau_{zz}) = \mu_n \left(\frac{\bar{u}_0}{h_0}\right)^{n-1} \left(\frac{\bar{u}_0}{l_0}\right) (\tau^*_{xx}, \tau^*_{zz}), \quad (\tau_{xz}, \tau_{zx}) = \mu_n \left(\frac{\bar{u}_0}{h_0}\right)^{n} (\tau^*_{xz}, \tau^*_{zx}), \tag{A 1c}$$

where h_0, l_0 and $\bar{u}_0$ are the characteristic depth, longitudinal length and longitudinal velocity scales respectively. The dimensionless conservation laws of mass and momentum are

$$\frac{\partial u^*}{\partial x^*}+\frac{\partial v^*}{\partial z^*}=0, \tag{A 2}$$

$$\frac{\partial u^*}{\partial t^*}+u^*\frac{\partial u^*}{\partial x^*}+v^*\frac{\partial u^*}{\partial z^*}=-\frac{\partial p^*}{\partial x^*}+\frac{\sin\theta}{Fr\,\epsilon}+\frac{\epsilon}{Re}\frac{\partial \tau^*_{xx}}{\partial x^*}+\frac{1}{Re\,\epsilon}\frac{\partial \tau^*_{zx}}{\partial z^*}, \tag{A 3}$$

$$\epsilon^2\left(\frac{\partial v^*}{\partial t^*}+u^*\frac{\partial v^*}{\partial x^*}+v^*\frac{\partial v^*}{\partial z^*}\right)=-\frac{\partial p^*}{\partial z^*}-\frac{\cos\theta}{Fr}+\frac{\epsilon}{Re}\frac{\partial \tau^*_{xz}}{\partial x^*}+\frac{\epsilon}{Re}\frac{\partial \tau^*_{zz}}{\partial z^*}, \tag{A 4}$$

where Re is the Reynolds number defined by (3.13),

$$Fr=\bar{u}_0^2/(gh_0) \tag{A 5}$$

and

$$\epsilon=\frac{h_0}{l_0}=\left(\frac{1+2n}{n}\right)^n\frac{1}{Re}. \tag{A 6}$$

The last equality is obtained by making use of (3.6), (3.11) and (3.12). The boundary conditions are

$$u^*=v^*=0 \quad \text{at} \quad z^*=0, \tag{A 7}$$

$$v^*=\frac{\partial h^*}{\partial t^*}+u^*\frac{\partial h^*}{\partial x^*} \quad \text{at} \quad z^*=h^*, \tag{A 8}$$

$$-\frac{\epsilon^2}{Re}\tau^*_{xx}\frac{\partial h^*}{\partial x^*}+\epsilon p^*\frac{\partial h^*}{\partial x^*}+\frac{1}{Re}\tau^*_{xz}=0 \quad \text{at} \quad z^*=h^*, \tag{A 9}$$

$$-\frac{\epsilon}{Re}\tau^*_{zx}\frac{\partial h^*}{\partial x^*}+\frac{\epsilon}{Re}\tau^*_{zz}-p^*=0 \quad \text{at} \quad z^*=h^*. \tag{A 10}$$

For long waves, we assume $\epsilon \ll 1$. Furthermore, we allow high-speed flows which satisfy

$$Fr \geqslant O(1), \quad \sin\theta/(Fr\,\epsilon)\sim O(1) \tag{A 11}$$

and

$$1/Re\,\epsilon \sim O(1). \tag{A 12}$$

Upon expanding the unknowns u^*, v^* and p^* in powers of ϵ, one can readily obtain (2.1)–(2.6) as the leading-order equations and boundary conditions in physical quantities. Note that the approximate equations for small Reynolds number $Re = O(1)$ are a subset of (2.1) and (2.2) with an $O(\epsilon^2)$ error.

Appendix B. Stability criterion for low Reynolds number

In this Appendix we shall deduce the linearized stability criterion for a steady uniform flow of a power-law fluid where $Re = O(1)$. From (A 3) and (A 4), we get

$$\epsilon\left(\frac{\partial u}{\partial t}+u\frac{\partial u}{\partial x}+v\frac{\partial u}{\partial z}+\frac{\cos\theta}{Fr}\frac{\partial h}{\partial x}\right)=\frac{\sin\theta}{Fr}+\frac{1}{Re}\frac{\partial}{\partial z}\left(\frac{\partial u}{\partial z}\right)^n+O(\epsilon^2). \tag{B 1}$$

On expanding the velocity components in powers of ϵ:

$$u=u_0+\epsilon u_1+\ldots, \quad v=v_0+\epsilon v_1+\ldots \tag{B 2}$$

we obtain from (A 2) and (B 1) the velocity profiles and the depth-averaged velocities: $O(1)$:

$$u_0 = \left(\frac{n}{1+n}\right)\left(\frac{Re\sin\theta}{Fr}\right)^{\frac{1}{n}}[h^{\frac{1+n}{n}} - (h-z)^{\frac{1+n}{n}}], \tag{B 3}$$

$$\bar{u}_0 = \left(\frac{n}{1+2n}\right)\left(\frac{Re\sin\theta}{Fr}\right)^{\frac{1}{n}} h^{\frac{1+n}{n}}; \tag{B 4}$$

$O(\epsilon)$:

$$u_1 = \frac{Re}{(1+n)^2}\left(\frac{Re\sin\theta}{Fr}\right)^{\frac{3-n}{n}} h_x h^{\frac{1}{n}}\left[h^{\frac{1+n}{n}}(h^{\frac{1+n}{n}} - (h-z)^{\frac{1+n}{n}}) - \frac{n}{2(1+2n)}(h^{\frac{2(1+n)}{n}} - (h-z)^{\frac{2(1+n)}{n}})\right]$$

$$- \frac{Re}{1+n}\left(\frac{Re\sin\theta}{Fr}\right)^{\frac{1-n}{n}} \frac{\cos\theta}{Fr} h_x (h^{\frac{1+n}{n}} - (h-z)^{\frac{1+n}{n}}) + O(\epsilon), \tag{B 5}$$

$$\bar{u}_1 = \frac{2Re}{(1+2n)(2+3n)}\left(\frac{Re\sin\theta}{Fr}\right)^{\frac{3-n}{n}} h_x h^{\frac{3+2n}{n}} - \frac{Re}{1+2n}\left(\frac{Re\sin\theta}{Fr}\right)^{\frac{1-n}{n}} \frac{\cos\theta}{Fr} h_x h^{\frac{1+n}{n}} + O(\epsilon). \tag{B 6}$$

Substituting $\bar{u}_0$ and $\bar{u}_1$ into the continuity equation

$$\frac{\partial h}{\partial t} + \frac{\partial(\bar{u}_0 h)}{\partial x} + \epsilon\frac{\partial(\bar{u}_1 h)}{\partial x} + O(\epsilon^2) = 0, \tag{B 7}$$

we get

$$h_t + \left(\frac{Re\sin\theta}{Fr}\right)^{\frac{1}{n}} h_x h^{\frac{1+n}{n}} + \epsilon\left\{\frac{2Re}{(1+2n)(2+3n)}\left(\frac{Re\sin\theta}{Fr}\right)^{\frac{3-n}{n}}\left(h_{xx}h^{\frac{3+3n}{n}} + \frac{3+3n}{n}h_x^2 h^{\frac{3+2n}{n}}\right)\right.$$

$$\left. - \frac{Re}{1+2n}\left(\frac{Re\sin\theta}{Fr}\right)^{\frac{1-n}{n}}\frac{\cos\theta}{Fr}\left(h_{xx}h^{\frac{1+2n}{n}} + \frac{1+2n}{n}h_x^2 h^{\frac{1+n}{n}}\right)\right\} + O(\epsilon^2) = 0. \tag{B 8}$$

The primary flow is steady and uniform and its depth and mean velocity are chosen as the characteristic depth and longitudinal velocity scales so that $h = 1$ and $\bar{u}_0 = 1$ and from (B 4),

$$\frac{Re\sin\theta}{Fr} = \left(\frac{1+2n}{n}\right)^n. \tag{B 9}$$

To study instabilities, we perturb the primary flow:

$$h = 1 + H \tag{B 10}$$

where $H = O(\mu) \ll 1$. Retaining only linear terms of the perturbations and making use of (B 9), we get from (B 8)

$$H_t + \left(\frac{1+2n}{n}\right)H_x + \epsilon\left\{\frac{2(1+2n)^2}{n^2(2+3n)} - \frac{\cos\theta}{Fr}\right\}\frac{Fr}{n\sin\theta}H_{xx} + O(\mu\epsilon^2) = 0. \tag{B 11}$$

Further assume normal mode disturbances

$$H = \mathrm{Re}\,(\hat{H}\exp[\mathrm{i}k(x-ct)]) \tag{B 12}$$

we obtain from (B 11)

$$-\mathrm{i}kc+\mathrm{i}\left(\frac{1+2n}{n}\right)k-\epsilon\left\{\frac{2(1+2n)^2}{n^2(2+3n)}-\frac{\cos\theta}{Fr}\right\}\frac{Fr}{n\sin\theta}k^2+O(\epsilon^2)=0. \tag{B 13}$$

If we expand $c = c_0+\epsilon c_1+\ldots$, we get from (B 13)

$$c_0 = \frac{1+2n}{n}, \tag{B 14}$$

$$c_1 = \mathrm{i}\frac{kFr}{n\sin\theta}\left(\frac{1+2n}{n^2}+\frac{1+2n}{n(2+3n)}-\frac{\cos\theta}{Fr}\right). \tag{B 15}$$

Therefore the phase speed for $k \sim 0$ is $(1+2n)/n$ which is the same as (4.15) for high Reynolds number, while the leading order of the growth rate of the disturbances is

$$\epsilon k\,\mathrm{Im}\,(c_1) = \epsilon\frac{k^2Fr}{n\sin\theta}\left(\frac{1+2n}{n^2}+\frac{1+2n}{n(2+3n)}-\frac{\cos\theta}{Fr}\right). \tag{B 16}$$

Therefore the flow will be linearly stable when $k > 0$ and

$$\frac{\cos\theta}{Fr} > \frac{1+2n}{n^2}+\frac{1+2n}{n(2+3n)}$$

or, upon using (B 9),

$$Re < \frac{((1+2n)/n)^n\cot\theta}{[(1+2n)/n^2]+(1+2n)/[n(2+3n)]}. \tag{B 17}$$

For Newtonian fluid, (B 17) reduces to $Re < \frac{5}{6}\cot\theta$ as has been obtained on solving the Orr–Sommerfeld equation by Benjamin (1957) and Yih (1963). Note that (B 17) differs from the criterion (4.11) for high Reynolds number by the presence of the second term $(1+2n)/[n(2+3n)]$ in the denominator. The ratio of the second term to the first term in the denominator of (B 17) is $n/(2+3n)$ which is $\frac{1}{5}$ for the Newtonian case and becomes smaller when n decreases. In other words, when the fluid is more shear-thinning, the stability criterion (4.11) for high Re, obtained with the crude velocity profile (2.9), becomes closer to the criterion (B 17) for low Re with the more accurate profiles (B 3) and (B 5).

Appendix C. The critical flow condition

In this Appendix we shall prove the necessary existence of the critical section and the monotonicity of the surface slope between successive shocks.

It is well-known in hydraulics that a supercritical flow changes to a subcritical flow only through a hydraulic jump. Dressler (1949) showed that in the profile of roll waves in a turbulent flow in an open-channel, there is a critical section, in the moving coordinate system, such that

$$Fr^2 \equiv (\bar{u}-c)^2/gh = 1 \tag{C 1}$$

in physical variables. Within each wavelength, there is a transition from a supercritical ($Fr > 1$) to a subcritical ($Fr < 1$) state. Mathematically, the critical condition (C 1) also

corresponds to the vanishing of the denominator of a profile equation similar to (5.3). Dressler further showed that the numerator of this profile equation must also vanish at the critical section where the profile maintains a finite steepness. We shall now establish the necessity of the critical flow section from the mathematical view point.

Let us first rewrite the two conservation laws (3.8) and (3.9) in a matrix form:

$$\frac{\partial w_i}{\partial t} + D_{ij}\frac{\partial w_j}{\partial x} = y_i, \tag{C 2}$$

where

$$w_i = \begin{pmatrix} h \\ \bar{u} \end{pmatrix} \tag{C 3}$$

$$D_{ij} = \begin{pmatrix} \bar{u} & h \\ (\beta-1)\,\bar{u}^2 h^{-1} + \alpha & (2\beta-1)\,\bar{u} \end{pmatrix}, \tag{C 4}$$

and

$$y_i = \begin{pmatrix} 0 \\ A(h)\,h^{-1} \end{pmatrix}. \tag{C 5}$$

The eigenvalues of D_{ij} are

$$\Lambda^{\pm} = \beta\bar{u} \pm [\beta(\beta-1)\,\bar{u}^2 + \alpha h]^{\frac{1}{2}}. \tag{C 6}$$

The discriminant in (C 6) is always positive, so the eigenvalues are real and distinct and the system is hyperbolic, as expected. Accordingly there exist two families of characteristics with local slopes

$$C^{\pm}: \quad (\mathrm{d}x/\mathrm{d}t)^{\pm} = \beta\bar{u} \pm [\beta(\beta-1)\,\bar{u}^2 + \alpha h]^{\frac{1}{2}}. \tag{C 7}$$

Shocks can result from the intersections of adjacent characteristics of the C^+ family. Consider a single wavelength of wave profile whose depth is h_1 at the left end and h_2 at the right end. By (5.21) that $q > 0$, whenever h increases, $\bar{u}$ will increase and from (C 7) so will the slope of the C^+ characteristics. The opposite will be true when h decreases. Therefore if part of the wavelength has a decreasing profile, the C^+ characteristics over this part will intersect each other as time goes on and a shock will be formed. This contradicts the smoothness required in the interior of the profile. Consequently the wave profile must be monotonically increasing from h_1 to h_2 and the slope of the C^+ characteristics will also increase monotonically from the left end to the right end of the profile. The discontinuities between individual profiles will remain stationary and

$$(\mathrm{d}x/\mathrm{d}t)_1^+ < c < (\mathrm{d}x/\mathrm{d}t)_2^+. \tag{C 8}$$

The above inequality implies the existence of a critical characteristic $C_c^+(h_c, \bar{u}_c)$ at each wavelength (where $h_1 < h_c < h_2$ and $\bar{u}_1 < \bar{u}_c < \bar{u}_2$) such that

$$(\mathrm{d}x/\mathrm{d}t)_c^+ = c. \tag{C 9}$$

The critical characteristic must be a straight line and separates other C^+ characteristics into two groups:

(i) those on the left side of C_c^+ (with $h_1 < h < h_c$, $\bar{u}_1 < \bar{u} < \bar{u}_c$)

$$(\mathrm{d}x/\mathrm{d}t)^+ < c; \tag{C 10}$$

(ii) those on the right side of C_c^+ (with $h_c < h < h_2$, $\bar{u}_c < \bar{u} < \bar{u}_2$)

$$(\mathrm{d}x/\mathrm{d}t)^+ > c. \tag{C 11}$$

Furthermore we may show that all characteristics in the C^- family are advancing more slowly than the shock. Since

$$\begin{aligned}\beta\bar{u}-[\beta(\beta-1)\bar{u}^2+\alpha h]^{\frac{1}{2}} &\leqslant \beta\bar{u}-[\beta(\beta-1)\bar{u}^2]^{\frac{1}{2}} \text{ (because } \alpha \geqslant 0)\\ &< \beta\bar{u}-[(\beta-1)^2\bar{u}^2]^{\frac{1}{2}}\\ &= \bar{u}\end{aligned}$$

but $$\bar{u} < c$$

it follows that $$\beta\bar{u}-[\beta(\beta-1)\bar{u}^2+\alpha h]^{\frac{1}{2}} < c$$

or $$(\mathrm{d}x/\mathrm{d}t)^- < c \quad \text{for all } C^- \text{ characteristics.} \tag{C 12}$$

Thus, relative to a shock, a disturbance to the flow will propagate only downstream if it is initially superimposed on the left side of the critical section, but will propagate both downstream and upstream if it is initially on the right side of the critical section. In hydraulics, flows exhibiting these two kinds of behaviour are classified as supercritical and subcritical respectively. More specifically, we obtain, by substituting (C 7) into (C 9), (C 10) and (C 11),

$$\beta\bar{u}+[\beta(\beta-1)\bar{u}^2+\alpha h]^{\frac{1}{2}} \begin{cases} < \\ = c \\ > \end{cases} \Leftrightarrow \begin{cases} \text{supercritical} \\ \text{critical} \\ \text{subcritical.} \end{cases} \tag{C 13}$$

The usual definitions for supercritical, critical and subcritical flows in hydraulics may be recovered as a particular case of (C 13). Let the velocity profile be uniform, or $\beta = 1$, then the three conditions in (C 13) are

$$(\alpha h)^{\frac{1}{2}} \begin{cases} < \\ = c-\bar{u} \\ > \end{cases} \Leftrightarrow \begin{cases} \text{supercritical} \\ \text{critical} \\ \text{supercritical.} \end{cases}$$

In physical variables, they become the familiar definitions

$$1 \begin{cases} < \\ = \dfrac{c-\bar{u}}{(gh\cos\theta)^{\frac{1}{2}}} \equiv Fr \\ > \end{cases} \Leftrightarrow \begin{cases} \text{supercritical} \\ \text{critical} \\ \text{subcritical.} \end{cases}$$

Now the flow is supercritical at $(h_1, \bar{u}_1)$, critical at $(h_c, \bar{u}_c)$ and subcritical at $(h_2, \bar{u}_2)$, so

$$\beta\bar{u}_1+[\beta(\beta-1)\bar{u}_1^2+\alpha h_1]^{\frac{1}{2}} < c, \tag{C 14a}$$

$$\beta\bar{u}_c+[\beta(\beta-1)\bar{u}_c^2+\alpha h_c]^{\frac{1}{2}} = c, \tag{C 14b}$$

$$\beta\bar{u}_2+[\beta(\beta-1)\bar{u}_2^2+\alpha h_2]^{\frac{1}{2}} > c. \tag{C 14c}$$

On substituting $\bar{u}$ from (5.2), (C 14b) can be written as

$$B(h_c) = (\beta-1)c^2-\beta q^2 h_c^{-2}+\alpha h_c = 0. \tag{C 15}$$

Hence h_c must be the only positive root of $B(h) = 0$. As a check, we may alternatively deduce the conditions (C 14a) and (C 14c) directly from the momentum conservation equation (5.13). It can further be shown from (5.13) and (C 15) that when either h_1 or h_2 is equal to h_c, the other one must also be equal to h_c, implying a uniform flow.

We next prove that $A(h)$ also vanishes $h = h_c$. A left eigenvector associated with Λ^+ is

$$(l_1^+, l_2^+) = ((\beta-1)\bar{u}^2h^{-1}+\alpha, \quad (\beta-1)\bar{u}+[\beta(\beta-1)\bar{u}^2+\alpha h)]^{\frac{1}{2}}). \tag{C 16}$$

Multiplying the system (C 2) by l_i^+ will give

$$l_1^+ \frac{\mathrm{d}h}{\mathrm{d}t} + l_2^+ \frac{\mathrm{d}\bar{u}}{\mathrm{d}t} = l_2^+ A(h) h^{-1} \quad \text{along } C^+ \text{ characteristics.} \tag{C 17}$$

In particular, the quantities h_c and $\bar{u}_c$ along the critical C^+ characteristic are invariant with time. Therefore

$$\frac{\mathrm{d}h}{\mathrm{d}t} = \frac{\mathrm{d}\bar{u}}{\mathrm{d}t} = 0 \quad \text{along the } C_c^+ \text{ characteristic,}$$

which implies that the right-hand side of (C 17) must vanish at $h = h_c$ and $\bar{u} = \bar{u}_c$:

$$l_2^+(h_c, \bar{u}_c) A(h_c) h_c^{-1} = 0.$$

Since $l_2^+(h_c, \bar{u}_c)$ is always positive, it follows that

$$A(h_c) = h_c - (ch_c^{-1} - qh_c^{-2})^n = 0. \tag{C 18}$$

Thus both $A(h)$ and $B(h)$ have to vanish at the critical section $h = h_c$. Consequently, $A(h) = 0$ will have two positive roots by virtue of the conditions that $q > 0$ and $A(h)$ vanishes at $h = h_c$. It can be checked that $h = h_c$ is the larger root by examining the profile slope at this section, by L'Hospital's rule,

$$\lim_{h \to h_c} \frac{\mathrm{d}h}{\mathrm{d}\xi} = \frac{A'(h_c)}{B'(h_c)}. \tag{C 19}$$

As the profile slope must be positive and $B'(h)$ is always greater than 0, it is necessary that

$$A'(h_c) > 0 \tag{C 20}$$

or h_c is the larger positive root of $A(h) = 0$. Clearly the surface slope $A(h)/B(h)$ is always positive as long as h is greater than the smaller root h_a.

Appendix D. Inequalities among h_c, $\langle h \rangle$, h_a

Note from figure 6 that for any $h > h_a$

$$A(h) \leqslant 0 \quad \text{if and only if} \quad h_c \geqslant h > h_a, \tag{D 1}$$

$$A(h) > 0 \quad \text{if and only if} \quad h > h_c. \tag{D 2}$$

By definition, $h = \langle h \rangle$ is a section within a profile, while h_c is so from Appendix C. We now wish to show that $h = 1$ is also an interior section of a profile by proving that

$$h_c > 1 \quad \text{if} \quad \langle h \rangle < 1 \tag{D 3}$$

and

$$h_c < 1 \quad \text{if} \quad \langle h \rangle > 1. \tag{D 4}$$

That is, either $h_c > 1 > \langle h \rangle$ or $h_c < 1 < \langle h \rangle$ must be true. From (5.3) and (5.26), it is readily seen that

$$A(\langle h \rangle) = \langle h \rangle - \langle h \rangle^{-2n}, \tag{D 5}$$

$$A(1) = 1 - (c - q)^n. \tag{D 6}$$

Now we consider two complementary cases.

(i) If $\langle h \rangle \leqslant 1$ then $c - q \geqslant 1$ from (5.26). It follows from (D 5) and (D 6) that

$$A(\langle h \rangle) \leqslant 0, \qquad A(1) \leqslant 0$$

and therefore from (D 1),

$$h_c \geqslant 1 \geqslant \langle h \rangle > h_a$$

which proves (D 3).

(ii) If $\langle h \rangle > 1$ then $c - q < 1$ from (5.26). It follows from (D 5) that

$$A(\langle h \rangle) > 0.$$

Hence, by (D 2),

$$\langle h \rangle > h_c$$

which implies, by (5.25) and (5.26),

$$(1+q)h_c^{-1} > h_c^{\frac{1+2n}{n}} - qh_c^{-1}$$

or $h_c < 1$ which is the same as (D 4).

Only in the special case of uniform flow will the equality sign in case (i) hold i.e. $h = 1 = \langle h \rangle$. Note in particular that the inequality $\langle h \rangle \neq 1$ does not violate mass conservation, since both the averaged depth of the roll wave ($= \langle h \rangle$) and the depth of the uniform flow ($= 1$) are normalized for the same discharge $\langle Q \rangle$. Note also that Ishihara *et al.* (1954) assumed for a Newtonian layer that the flow quantities at the critical section are always equal to those of the corresponding uniform flow; this is incorrect.

REFERENCES

ALEKSEENKO, S. V., NAKORYAKOV, V. YE. & POKUSAEV, B. G. 1985 Wave formation on a vertical falling liquid film. *AIChE J.* **31**, 1446–1460.

BENJAMIN, T. B. 1957 Wave formation in laminar flow domain an inclined plane. *J. Fluid Mech.* **2**, 554–574.

BRYANT, A. E. J. & WILLIAMS, D. J. A. 1980 Rheology of cohesive suspensions. In *Industrialized Embayments and Their Environmental Problems* (ed. M. B. Collins) Pergamon.

CHANG, H.-C., DEMEKHIN, E. A. & KOPELEVICH, D. I. 1993 Nonlinear evolution of waves on a vertically falling film. *J. Fluid Mech.* **250**, 433–480.

CORNISH, V. 1934 *Ocean Waves and Kindred Geophysical Phenomena.* Cambridge University Press.

DAI, J., WAN, Z., WANG, W., CHENG, W. & LI, X. 1980 An experimental study of slurry transport in pipes. In *Proc. Intl Symp. River Sedimentation, Beijing, China*, Vol. 1, pp. 195–204 (in chinese).

DARBY, R. 1986 Laminar and turbulent pipe flows of non-Newtonian fluids. In *Encyclopedia of Fluid Mechanics*, Vol. 7 (ed. N. P. Cheremisinoff), pp. 19–53. Gulf.

DAVIES, T. R. H. 1986 Large debris flows: a macro-viscous phenomenon. *Acta Mechanica* **63**, 161–178.

DRESSLER, R. F. 1949 Mathematical solution of the problem of roll-waves in inclined open channels. *Commun. Pure Appl. Maths* **2**, 149–194.

DRESSLER, R. F. & POHLE, F. V. 1953 Resistance effects on hydraulic instability. *Commun. Pure Appl. Maths* **6**, 93–96.

HWANG, S.-H. & CHANG, H.-C. 1987 Turbulent and inertial roll waves in inclined film flow. *Phys. Fluids* **30**, 1259–1268.

ISHIHARA, T., IWAGAKI, Y. & IWASA, Y. 1954 Theory of the roll wave train in laminar water flow on a steep slope surface. *Trans. JSCE* **19**, 46–57 (in Japanese).

JEFFREYS, H. 1925 The flow of water in an inclined channel of rectangular section. *Phil. Mag.* **49** (6), 793–807.

JOHNSON, A. M. 1970 *Physical Processes in Geology.* Freeman, Cooper and Co.

JULIEN, P. Y. & HARTLEY, D. M. 1985 Formation of roll waves in laminar sheet flow. *Rep.* CER84-85PYJ-DMH18, Department of Civil Engineering, Colorado State University.

JULIEN, P. Y. & HARTLEY, D. M. 1986 Formation of roll waves in laminar sheet flow. *J. Hydraul. Res.* **24**, 5–17.

KAJIUCHI, T. & SAITO, A. 1984 Flow enhancement of laminar pulsating flow of Bingham plastic fluids. *J. Chem. Engng Japan* **17**, 34–38.

KAPITZA, P. L. 1948 Wave flow of thin layers of a viscous fluid. *Zh. Eksp. Teor. Fiz.* **18**, 3–28. (See also *Collected Papers of P. L. Kapitza, Vol. II, 1938–1964*, Pergamon Press (1965), pp. 662–709.)

LI, J., YUAN, J., BI, C. & LUO, D. 1983 The main features of the mudflow in Jiang-jia Ravine. *Zeit. Geomorph.* **27**, 325–341.

LIU, J., PAUL, J. D. & GOLLUB, J. P. 1993 Measurements of the primary instabilities of film flows. *J. Fluid Mech.* **250**, 69–101.

LIU, K. F. 1990 Dynamics of a shallow layer of fluid mud. PhD thesis, Civil Engineering Department, MIT.

MAYER, P. G. 1959 Roll waves and slug flows in inclined open channels. *J. Hydraul. Div., ASCE* **85** (HY7), 99–141.

MERKIN, J. H. & NEEDHAM, D. J. 1986 An infinite period bifurcation arising in roll waves down an open inclined channel. *Proc. R. Soc. Lond.* A **405**, 103–116.

NEEDHAM, D. J. 1988 The development of a bedform disturbance in an alluvial river of channel. *Z. Angew. Math. Phys.* **39**, 28–49.

NEEDHAM, D. J. 1990 Wave hierarchies in alluvial river flows. *Geophys. Astrophys. Fluid Dyn.* **51**, 167–194.

NEEDHAM, D. J. & MERKIN, J. H. 1984 On roll waves down an open inclined channel. *Proc. R. Soc. Lond.* A **394**, 259–278.

O'BRIEN, J. S. & JULIEN, P. Y. 1988 Laboratory analysis of mudflow properties. *J. Hydraul. Engng ASCE* **114** (8), 877–887.

OKUDA, S., SUWA, H., OKUNISHI, K., YOKOYAMA, K. & NAKANO, M. 1980 Observations on the motion of a debris flow and its geomorphological effects. *Zeit. Geomorph.* Suppl.-Bd. **35**, 142–163.

PIERSON, T. C. 1980 Erosion and deposition by debris flows at Mt Thomas, North Canterbury, New Zealand. *Earth Surf. Proc.* **5**, 227–247.

PROKOPIOU, TH., CHENG, M. & CHANG, H.-C. 1991 Long waves on inclined films at high Reynolds number. *J. Fluid Mech.* **222**, 665–691.

QIAN, N. & WAN, Z. 1986 *A Critical Review of the Research on the Hyperconcentrated Flow in China.* International Research and Training Centre on Erosion and Sedimentation, Beijing, China.

SCHLICHTING, H. 1979 *Boundary-Layer Theory*. McGraw Hill.

SHARP, R. P. & NOBLES, L. H. 1953 Mudflow of 1941 at Wrightwood, southern California. *Geol. Soc. Am. Bull.* **64**, 547–560.

TAMADA, K. & TOUGOU, H. 1979 Stability of roll waves on thin laminar flow down an inclined plane wall. *J. Phys. Soc. Japan* **47**, 1992–1998.

TANNER, R. I. 1985 *Engineering Rheology*. Clarendon.

WAN, Z. 1982 Bed material movement in hyperconcentrated flow. *Series Paper* 31. Inst. Hydrodynamics and Hydraulic Engineering, Technical University of Denmark.

WHITHAM, G. B. 1974 *Linear and Nonlinear Waves*. John Wiley & Sons.

YANO, K. & DAIDO, A. 1965 Fundamental study on mudflows. *Ann. Disaster Prevention Res. Inst., Kyoto Univ.* **7**, 340–347.

YIH, C.-S. 1963 Stability of liquid flow down an inclined plane. *Phys. Fluids* **6**, 321–334.